JCTC Journal of Chemical Theory and Computation

Article

pubs.acs.org/JCTC

New Interaction Parameters for Charged Amino Acid Side Chains in the GROMOS Force Field

Maria M. Reif,[†] Philippe H. Hünenberger,[‡] and Chris Oostenbrink*,[†]

[†]Institute for Molecular Modeling and Simulation, University of Natural Resources and Life Sciences, 1190 Vienna, Austria

[‡]Laboratory of Physical Chemistry, Swiss Federal Institute of Technology (ETH), 8093 Zurich, Switzerland

Supporting Information

ABSTRACT: A GROMOS force-field parameter set 54A8 is developed, which is based on the latest 54A7 set [Schmid et al. *Eur. Biophys. J.* **2011**, *40*, 843−856] and involves a recalibration of the nonbonded interaction parameters for the charged amino acid side chains, based on ionic side chain analogs. After a thorough analysis of the available experimental data, conventional hydration free energies for the ammonium; mono-, di-, tri-, and tetramethyl-ammonium; formate; acetate; propanoate; imidazolium; and guanidinium ions are combined with a standard absolute intrinsic proton hydration free energy $\Delta G^{\ominus}_{hyd}[H^{+}_{g}] = -1100$ kJ·mol^{-1} to yield absolute intrinsic single-ion hydration free energies serving as experimental target data. The raw hydration free energies calculated from atomistic simulations are affected by electrostatic and finite-size artifacts, and corrections are applied to reach methodological independence prior to comparison with these experimental values. Except for monomethyl-ammonium, ions with parameters derived directly from the 54A7 force field considerably underestimate (ammonium, formate, acetate, propanoate, guanidinium) or overestimate (di-, tri-, and tetramethyl-ammonium; imidazolium) the magnitude of the intrinsic hydration free energy, the largest deviation affecting the acetate ion (40.0 kJ·mol^{-1}). After reparameterization into 54A8, the mean and maximal absolute deviations between simulated and experimental data over the set of 10 ions are reduced from 23.1 and 40.0 kJ·mol^{-1}, respectively, to 1.8 and 6.3 kJ·mol^{-1}, respectively. Although the 54A7 and 54A8 parameter sets differ significantly in terms of the hydration free energies of the ions considered, other properties such as ion−water radial distribution functions and ion−ion potentials of mean force appear to be only moderately sensitive to this change. These properties are similar for the two sets and, in the case of the ion−water radial distribution functions, in good agreement with available experimental data.

I. INTRODUCTION

During past decades, classical atomistic simulation has established itself as a powerful method to study molecular structure, thermodynamics, and dynamics at a resolution often inaccessible to experiment.[1−4] It is widely applied in various areas of the natural sciences to complement experimental measurements or predict experimental properties for complex (bio)-molecular systems.

The atomistic representation considers individual atoms of the system, exempt of distinct electronic and nuclear components, as mass-possessing point particles associated with a unique interaction site, and relies on statistical mechanics to calculate the thermodynamic properties of a macroscopic system from an ensemble of Boltzmann-weighted configurations which are generated numerically, e.g., using a molecular dynamics (MD) integration scheme. The forces acting on the atoms are derived from an empirical classical potential-energy function (force field), which is defined by its functional form and associated parameters. The parameters of a force field are calibrated by comparison of simulated observables against experimental or/and quantum-mechanical target data. Their applicability is restricted to given pressure and temperature conditions, to a given type of phase, and to a given simulation methodology. These restrictions may be due to the specific choice of target data (e.g., the thermodynamic state point and phase it pertains to) or to various approximations involved in the simulation methodology (e.g., cutoff truncation or artificial periodicity), in the force-field functional form (e.g., implicit description of electronic polarizability), and in the force-field complexity (e.g., use of combination rules).[4]

The GROMOS force field[5−13] is a united-atom implict-polarization force field appropriate for the simulation of (bio)molecular systems close to $P^{\circ} = 1$ bar and $T^{-} = 298.15$ K in the condensed phase. Its underlying construction and parametrization principles have recently been summarized elsewhere,[12,13] and only those of prime relevance to the present study will be repeated here.

Concerning the construction of the force field, these are (*i*) a united-atom representation of aliphatic CH_n (n = 1, 2, 3, 4) groups; (*ii*) a Lennard-Jones (12-6 function[14−16]) representation of van der Waals interactions; (*iii*) a geometric-mean combination rule[6] to define heteroatomic Lennard-Jones interaction parameters based on homoatomic ones; (*iv*) an implicit (mean-field) representation of electronic polarization effects through charge enhancement; (*v*) an independent definition of atomic partial charges and Lennard-Jones atom types. Concerning the parametrization of the force field, these are (*i*) the desire to preserve the simplicity of the force field, within the limits imposed by the complexity of the systems it is intended to describe; (*ii*) the optimization of parameters for small molecules (e.g., amino acid side chain analogs) and their

Special Issue: Wilfred F. van Gunsteren Festschrift

Received: February 22, 2012
Published: April 11, 2012

subsequent transfer to larger entities (e.g., proteins); (*iii*) the focus on experimental thermodynamic condensed-phase properties during the parametrization procedure; (*iv*) the compatibility of the parameters with the simple-point-charges (SPC) water model;[17] (*v*) the compatibility of the parameters with cutoff-truncated electrostatic interactions (cutoff distance of 1.4 nm) including a Barker–Watts reaction-field correction.[18]

The first parameter set[5] of the GROMOS force field dates back to 1984 (26C1; see also ref 19 for an earlier study using this set). Throughout the years, a number of revised and extended sets have been published, e.g., involving an improved description of aliphatic hydrocarbons,[6−8,20] lipids,[21] small molecules including in particular neutral amino acid side chain analogs,[10] nucleic acids,[22] hexapyranose-based carbohydrates,[9,11] oxygen-containing compounds,[12] and amides.[23] The 53A5 force field[10] was developed for an accurate description of the thermodynamic properties of pure liquids. Since it did not seem possible at that time to reconcile both pure-liquid and hydration properties with a sufficient accuracy, the 53A6 force field[10] aimed primarily at reproducing solvation properties of (neutral) amino acid side chain analogs in aqueous and nonaqueous solvents. The $53A6_{OXY}$ parameter set[12] strikes a balance between the 53A5 and 53A6 versions, by providing a single set to reproduce pure-liquid properties and solvation free energies of small oxygen-containing molecules. The 54A7 force field version[13] is based on 53A6, with a number of force-field adjustments, namely, (*i*) the use of new peptide ϕ, ψ torsional-angle energy terms, in combination with a slightly reduced Lennard-Jones repulsion between the backbone oxygen and nitrogen atom types; (*ii*) the introduction of a new atom type for the methyl group in a positively charged entity, as e.g. found in the choline headgroup of phosphatidylcholine lipids;[24] (*iii*) a change of the Lennard-Jones interaction parameters of the sodium and chloride ions.[25] The present work is based on the 54A7 force field, but the reoptimized parameters proposed here could be used within $53A6_{OXY}$ as well since they do not concern atom types differing between the two versions.

One noteworthy deficiency of the GROMOS 54A7 force field is the parametrization of charged amino acid side chains, which was continuously adopted from previous force-field versions and is thus unchanged since 1984, except for some modifications in the Lennard-Jones interaction parameters that were never validated for these specific side chains. However, the original parametrization of 1984 was not based on a rigorous comparison between calculated hydration free energies and experimental data, but essentially relied on chemical intuition alone. Until recently, this parametrization strategy may have been justified by the notorious difficulties associated with the experimental and theoretical determination of absolute intrinsic single-ion hydration free energies.[4] These difficulties have two fundamental causes: (*i*) due to the absence of free gas-phase ions at equilibrium and the presence of a surface polarization at the air–water interface, absolute intrinsic single-ion hydration free energies are experimentally elusive quantities, i.e., their determination always requires the introduction of an extra-thermodynamic assumption; (*ii*) due to limitations in the computing power, simulated systems are of truly microscopic sizes, so that calculated single-ion hydration free energies are highly sensitive to the chosen spatial boundary conditions (i.e., shape, size, treatment of the surroundings or artificial periodicity of the system) and to the approximate treatment of the electrostatic interactions (e.g., cutoff-truncation, finite-size, and surface effects), thus causing a strong dependence of the results on the employed simulation methodology (see refs 4, 25, 26, and references therein).

Nowadays, however, the intricate experimental, theoretical, and conceptual issues afflicting the field of single-ion solvation thermodynamics are better understood.[4] Many studies[4,25,27−32] suggest that the best estimate to date for the standard absolute intrinsic hydration free energy $\Delta G^{\ominus}_{hyd}[H_g^+]$ of the proton is that of Tissandier et al.[33,34] (-1104.5 kJ·mol^{-1}), derived from conventional values and experiments on ion–water clusters in the gas phase, without correction from Boltzmann to Fermi–Dirac statistics for the standard-state electron[35,36] (corrected value of[35] -1100.9 kJ·mol^{-1}). Furthermore, raw results for ionic charging free energies calculated using atomistic simulations can nowadays be corrected *ex post*[4,25,26,37,38] so that methodological independence is achieved, thus permitting a reliable calculation of absolute intrinsic single-ion solvation free energies.

These accomplishments make it possible to reliably optimize the parameters required for the force-field representation of ionic compounds (atomic partial charges and Lennard-Jones interaction parameters) in such a way that agreement between calculated and experimental intrinsic single-ion hydration free energies is reached. Such a calibration approach is not new and has been applied many times in the past, principally in the context of monatomic ions (see e.g. Suppl. Mat. I of ref 25 for an overview). However, prior to the establishment of consensus experimental estimates for intrinsic single-ion hydration free energies and the design of a consistent scheme for correcting the methodology dependence of the simulation results,[26,38] unreliable target data and inaccurate corrections were employed, which may heavily impair the quality of the resulting parameter sets.

For monatomic ions, the Lennard-Jones repulsion parameter is typically the only degree of freedom subject to calibration against the hydration free energy,[25] the ionic charge being unambiguous and the Lennard-Jones dispersion parameter being conveniently derived on the basis of approximate formulas relating it to the ionic polarizability.[4,25,39] In contrast, the parametrization of polyatomic ions is an underdetermined problem; i.e., it allows for multiple solutions of similar quality with respect to the reproduction of a single experimental value. This is due to the multiplicity of atomic partial charges and Lennard-Jones repulsion parameters, as well as to the loss of a direct connection between dispersion parameters and atomic polarizabilities, the latter being ill-defined when considering (united) atoms within molecules. For this reason, reaching agreement between calculated and experimental hydration free energies as outlined above may represent a very deceptive assessment of the quality of the corresponding force-field representation, and it is essential to perform further validation against other properties.

Valuable quantities to validate against would be, e.g., solvation free energies in nonaqueous solvents. However, because experimental data for the solvation of ions in such solvents is rather sparse, it is generally very difficult to make an unambiguous suggestion for the corresponding absolute intrinsic proton solvation free energy. In addition, the calculation of methodology-independent ionic solvation free energies in solvents involving multiple Lennard-Jones interaction sites is a tedious procedure for monatomic ions (manuscript in preparation), and even more so for polyatomic ones. In water, comparison against ion–solvent radial distribution functions inferred from neutron diffraction experiments offers one

possible validation route. However, these functions are typically moderately sensitive to the force-field parameters and, because they are derived observables, also affected by experimental uncertainties and ambiguities. Considering the role of the charged amino acid side chains in proteins and of the charged amino acid side chain analogs in solution, another important property to validate against is the ion−ion association behavior. This is crucial for the accurate description of salt bridges in proteins or of Hofmeister effects,[40−46] e.g., salting-in vs salting-out behavior concerning the effect on biomacromolecules, cosmotropic vs chaotropic behavior concerning the effect on the solvent structure, and high vs low solubility of a given salt concerning the effect on the dissociation equilibrium. Experimental data on ion−ion interactions in aqueous solution are also available in the form of activity coefficients for electrolyte solutions at finite concentrations. These can be related to ion−ion radial distribution functions *via* Kirkwood−Buff theory[47,48] and used as validation data for ion−solvent interaction parameters. Note that this approach has also been commonly applied in the recent past for force-field calibration purposes.[49,50] However, it raises issues concerning the appropriateness of combination rules, which are not involved in the hydration free energy approach (present work), and concerning the generally very large dependence of the calculated ion−ion radial distribution functions on the employed electrostatic interaction scheme.

The present study focuses on the calculation of the intrinsic single-ion hydration free energies of the ions (Table 1)

Table 1. Abbreviations Used for the Names of the Different Ions Throughout the Article

ion name	formula	abbreviation
ammonium	NH_4^+	H4C0
monomethyl-ammonium	$H_3NCH_3^+$	H3C1
dimethyl-ammonium	$H_2N(CH_3)_2^+$	H2C2
trimethyl-ammonium	$HN(CH_3)_3^+$	H1C3
tetramethyl-ammonium	$N(CH_3)_4^+$	H0C4
formate	$HCOO^-$	FORM
acetate	CH_3COO^-	ACET
propanoate	$CH_3CH_2COO^-$	PROP
imidazolium	ring(−CH−NH−CH−NH−CH−)$^+$	IMID
guanidinium	$C(NH_2)_3^+$	GUAN
sodium	Na^+	NA
chloride	Cl^-	CL

ammonium (H4C0), methyl-ammonium (H3C1; of relevance for the charged lysine side chain), dimethyl-ammonium (H2C2), trimethyl-ammonium (H1C3), tetramethyl-ammonium (H0C4; of relevance for the choline headgroup of phosphatidylcholine lipids), formate (FORM), acetate (ACET), propanoate (PROP; of relevance for the aspartate and glutamate side chains), imidazolium (IMID; of relevance for the charged histidine side chain), and guanidinium (GUAN; of relevance for the charged arginine side chain) and the characterization of the solvation structure and interionic association properties of these ions in the infinitely dilute regime. Its aim is threefold, namely:

1. assessing the quality of the description of charged amino side chain analogs in the 54A7 force field by calculating the corresponding intrinsic single-ion hydration free energies
2. reoptimizing the atomic partial charges and, if necessary, the Lennard-Jones interaction parameters of 54A7 into a new set 54A8, based on carefully chosen experimental data for intrinsic single-ion hydration free energies and calculated hydration free energies including appropriate corrections for methodological errors
3. performing an initial validation of the new 54A8 set against properties other than single-ion hydration free energies, namely, ion−water radial distribution functions (RDFs) and ion−ion potentials of mean force (PMFs), the former being compared to experimental results and the latter to corresponding results for the 54A7 set

II. Methods.

II.1. Experimental Data for Single-Ion Hydration Free Energies.

II.1.1. General Considerations. Due to the presence of a surface polarization at the air−water interface, the absolute intrinsic single-ion hydration free energy $\Delta G^{\ominus}_{hyd}[I^z_g]$ of a gas-phase ion I^z_g, z denoting the signed integer charge, is an experimentally elusive quantity, i.e., its determination requires the introduction of an extra-thermodynamic assumption.[4] Although the contribution of the air−water interfacial potential cancels out when considering overall neutral sets of ions, the hydration free energy $\Delta G^{\ominus}_{hyd}[I^z_g + J^{-z}_g]$ of a neutral gas-phase ion pair, i.e., the sum over the corresponding free energies for the individual I^z_g and J^{-z}_g species, is not directly accessible experimentally either, due to the absence of free gaseous ions at equilibrium.[4] However, a thermodynamic cycle involving atomization, ionization, solvation, and reformation processes

$$I_{el} + J_{el} \rightarrow I_g + J_g \rightarrow I^z_g + J^{-z}_g \rightarrow I^z_{aq} + J^{-z}_{aq} \rightarrow I_{el} + J_{el} \quad (1)$$

where el, g, and aq denote element standard-state, gaseous, and aqueous species, respectively, may be applied. The hydration free energy $\Delta G^{\ominus}_{hyd}[I^z_g + J^{-z}_g]$ of the gas-phase ion pair is then deduced from the formation free energy $\Delta G^{\ominus}_f[I^z_{aq} + J^{-z}_{aq}]$ of the dissolved salt, the atomization (gas-phase atom formation) free energies $\Delta G^{\ominus}_a[I_{el}] + \Delta G^{\ominus}_a[J_{el}]$ of the element pair, and the ionization free energies $\Delta G^{\ominus}_i[I_g] + \Delta G^{\ominus}_i[J_g]$ of the gas-phase atom pair as[4]

$$\begin{aligned}\Delta G^{\ominus}_{hyd}[I^z_g + J^{-z}_g] = &-(\Delta G^{\ominus}_a[I_{el}] + \Delta G^{\ominus}_i[I_g]) \\ &- (\Delta G^{\ominus}_a[J_{el}] + \Delta G^{\ominus}_i[J_g]) \\ &+ \Delta G^{\ominus}_f[I^z_{aq} + J^{-z}_{aq}]\end{aligned} \quad (2)$$

where the notations $I^z_g + J^{-z}_g$ and $I^z_{aq} + J^{-z}_{aq}$ represent a sum of thermodynamic parameters appropriate for the separate I^z_g and J^{-z}_g or I^z_{aq} and J^{-z}_{aq} species, respectively.

The partitioning of the salt hydration free energies determined in this way results in a set of single-ion parameters defined within an unknown constant, weighted by the integer charge of the ion. For this reason, single-ion hydration free energies are usually tabulated on relative (conventional) scales, where the hydration free energy for a specific ion is set to a given constant by definition. Most commonly, the hydration free energy of the proton is set to zero. The standard conventional hydration free energy $\Delta G^{\bullet}_{hyd}[I^z_g]$ of an ion I^z_g is then connected to the corresponding standard absolute intrinsic hydration free energy $\Delta G^{\ominus}_{hyd}[I^z_g]$ as

$$\Delta G^{\ominus}_{hyd}[I^z_g] = \Delta G^{\bullet}_{hyd}[I^z_g] + z\Delta G^{\ominus}_{hyd}[H^+_g] \quad (3)$$

dx.doi.org/10.1021/ct300156h | J. Chem. Theory Comput. 2012, 8, 3705−3723

Table 2. Experimental Data for Gas-Phase (I^z_g, AH^+_g) and Aqueous (I^z_{aq}, AH^+_{aq}) Ions Used in the Calculation of Standard Conventional ($\Delta G^{\bullet}_{hyd}[I^z_g]$ or $\Delta G^{\bullet}_{hyd}[AH^+_g]$) and Intrinsic ($\Delta G^{\ominus}_{hyd}[I^z_g]$ or $\Delta G^{\ominus}_{hyd}[AH^+_g]$) Single-Ion Hydration Free Energies[a]

		notes	ref.
	H4C0		
$\Delta G^{\boxminus,alt}_{hyd}[I^z_g]$	−356.5		32
$\Delta G^{\bullet}_{hyd}[I^z_g]$	756.1	*b*	32
$\Delta G^{\ominus}_{hyd}[I^z_g]$	−344.0	*c*	this work
	H3C1		
$\Delta G^{\boxminus,alt}_{hyd}[I^z_g]$	−319.7		32
$\Delta G^{\bullet}_{hyd}[I^z_g]$	792.9	*b*	32
$\Delta G^{\ominus}_{hyd}[I^z_g]$	−307.1	*c*	this work
	H2C2		
$\Delta G^{\boxminus,alt}_{hyd}[I^z_g]$	−287.0		32
$\Delta G^{\bullet}_{hyd}[I^z_g]$	825.5	*b*	32
$\Delta G^{\ominus}_{hyd}[I^z_g]$	−274.5	*c*	this work
	H1C3		
$\Delta G^{\boxminus,alt}_{hyd}[I^z_g]$	−255.6		32
$\Delta G^{\bullet}_{hyd}[I^z_g]$	856.9	*b*	32
$\Delta G^{\ominus}_{hyd}[I^z_g]$	−243.1	*c*	this work
	H0C4		
$\Delta_f H^{\bullet}\ [I^z_{aq}]$	−105.2		53
$\Delta_f H^{(\ominus)}\ [I^z_g]$	546.0		53
$\Delta_f H^{\ominus}[I^z_g]$	542.9	*d*	
$\Delta H^{\bullet}_{hyd}[I^z_g]$	885.0	*e*	
$s^{\ominus}[I^z_g]$	331.9		54
$s^{\ominus,alt}[I^z_{aq}]$	187.8		54
$s^{\bullet}[I^z_{aq}]$	210.0	*f*	54
$\Delta S^{\bullet}_{hyd}[I^z_g]$	−13.0	*g*	
$\Delta G^{\bullet}_{hyd}[I^z_g]$	888.9	*h*	
$\Delta G^{\ominus}_{hyd}[I^z_g]$	−211.1	*c*	this work
	FORM		
$\Delta G^{\boxminus,alt}_{hyd}[I^z_g]$	−318.8		32
$\Delta G^{\bullet}_{hyd}[I^z_g]$	−1415.4	*b*	32
$\Delta G^{\ominus}_{hyd}[I^z_g]$	−315.4	*c*	this work
	ACET		
$\Delta G^{\boxminus,alt}_{hyd}[I^z_g]$	−324.7		32
$\Delta G^{\bullet}_{hyd}[I^z_g]$	−1421.2	*b*	32
$\Delta G^{\ominus}_{hyd}[I^z_g]$	−321.2	*c*	this work
	PROP		
$\Delta G^{\boxminus,alt}_{hyd}[I^z_g]$	−318.8		32
$\Delta G^{\bullet}_{hyd}[I^z_g]$	−1415.4	*b*	32
$\Delta G^{\ominus}_{hyd}[I^z_g]$	−315.4	*c*	this work
	IMID		
$GB[A_g]$	909.2		57
$pK_a[AH^+_{aq}]$	7.0		58, 62
$\Delta G^{\ominus}_{hyd}[A_g]$	−33.1	*i*	61
$\Delta G^{\bullet}_{hyd}[AH^+_g]$	836.1	*j*	
$\Delta G^{\ominus}_{hyd}[AH^+_g]$	−263.9	*c*	this work
	GUAN		
$GB[A_g]$	949.4		57
$pK_a[AH^+_{aq}]$	13.6−13.8	*k*	58, 62, 112, 113
$\Delta G^{\ominus}_{hyd}[A_g]$	-(−38.9)	*l*	60
$\Delta G^{\bullet}_{hyd}[AH^+_g]$	-(832.9, 832.3, 831.7)	*j*, *m*	
$\Delta G^{\ominus}_{hyd}[AH^+_g]$	−269.0 (−267.1, −267.7, −268.3)	*c*, *m*, *n*	this work

[a]The notation I^z refers to an ion of signed integer charge *z*. The notation AH^+ is used for the protonated species IMID and GUAN. See Sections II.1.1−II.1.4 for details. Abbreviations for the ion names are defined in Table 1. [b]Equation 5, using $\Delta G^{\boxminus,alt}_{hyd}[H^+_g] = -1112.5$ kJ·mol^{-1} and $\Delta G^{\ominus}_{std} = 7.95$ kJ·mol^{-1}. [c]Equation 3, using $\Delta G^{\ominus}_{hyd}[H^+_g] = -1100$ kJ·mol^{-1}. [d]Equation 7, using $\Delta_f H^{(\ominus)\to\ominus} = -3.1$ kJ·mol^{-1}. [e]Equations 9 and 10, using $\Delta_f H^{\ominus}[H^+_g] = 1533.1$ kJ·mol^{-1}. [f]Equation 11, using $s^{\ominus,alt}[H^+_{aq}] = -22.2$ J·mol^{-1}·K^{-1}. [g]Equations 12 and 13, using $s^{\ominus}[H^+_g] = 108.95$ J·mol^{-1}·K^{-1}. [h]Equation 6. [i]The value reported in the original source refers to equal concentrations in the gas and aqueous phases and was converted to a standard hydration free energy according to eq 4 with $\Delta G^{\ominus}_{std} = 7.95$ kJ·mol^{-1}. [j]Equation 14. [k]Refs 62, 112, and 58 report pK_a values in dilute solution of 13.6 (25 °C), 13.71 (20 °C) and 13.8 (25 °C), respectively, while ref 113 reports a pK_a value in 6 M (molar) solution of 13.74 (25 °C). [l]The value reported between parentheses refers to methylguanidine[60] (A_g). [m]The three values reported between parentheses are based on the $\Delta G^{\ominus}_{hyd}[A_g]$ for methylguanidine, along with pK_a values of 13.6, 13.7 and 13.8, respectively. [n]The value for guanidinium is inferred based on a pK_a value of 13.7 and on $\Delta G^{\ominus}_{hyd}[A_g]$ for methylguanidine after removal of 1.3 kJ·mol^{-1} as an estimated increment for the methyl group.

where $\Delta G^{\ominus}_{hyd}[H^+_g]$ is the standard absolute intrinsic hydration free energy of the proton.

The force-field parametrization work performed in this study relies on single-ion hydration free energies that are intrinsic. Intrinsic quantities exclusively characterize the interaction of the ion with bulk water, i.e., do not, as opposed to so-called real quantities, intermingle bulk and surface contributions. The corresponding experimentally unambiguous conventional hydration free energy data are anchored into an absolute intrinsic scale based on a recommended[4,25] value $\Delta G^{\ominus}_{hyd}[H^+_g] = -1100$ kJ·mol^{-1} for the standard absolute intrinsic hydration free energy of the proton. The standard states are defined throughout this study by a reference pressure $P^\circ = 1$ bar, a reference temperature $T^= = 298.15$ K, a reference concentration $b^\circ = 1$ m (1 molal) for the aqueous phase, and a standard state for the free electron according to the warm-electron convention (ideal-gas at temperature $T^=$, according to Fermi−Dirac statistics; Fermi−Dirac statistics is also applied for the gas-phase standard state of the proton).[4]

The results directly obtained from free-energy calculations based on atomistic simulations are typically not standard. They correspond to an intrinsic point-to-point hydration free energy $\Delta G^{\boxminus}_{hyd}[I^z_g]$ characterizing the transfer of the ion from a fixed point in the gas phase to a fixed point in bulk water, excluding the contribution of surface crossing. This is equivalent to a hydration free energy characterizing a transfer from a given volume in the gas phase to the same effective volume in water, i.e., corresponds to the same reference concentrations in the gas and aqueous phases. Conversion of $\Delta G^{\boxminus}_{hyd}[I^z_g]$ to the corresponding standard quantity $\Delta G^{\ominus}_{hyd}[I^z_g]$, which characterizes a transfer from a random location within the molar volume accessible to the ion in the ideal gas at pressure P° and temperature $T^=$ to a random location within the molar volume accessible to the aqueous ion in an ideal solution at pressure P°, molality b°, and temperature $T^=$, is given by[4]

$$\Delta G^{\ominus}_{hyd}[I^z_g] = \Delta G^{\boxminus}_{hyd}[I^z_g] + \Delta G^{\ominus}_{std} \quad (4)$$

where $\Delta G^{\ominus}_{std} = RT^= \ln[(P^\circ)^{-1}RT^=b^\circ\rho^{\ominus}_w]$, $\rho^{\ominus}_w$ being the density of pure water at pressure P° and temperature $T^=$, and R the ideal-gas constant. Using[51] $\rho^{\ominus}_w = 997$ kg·m^{-3}, the standard-state conversion term $\Delta G^{\ominus}_{std}$ evaluates to 7.95 kJ·mol^{-1}.

The three following sections outline how experimental data were obtained for the standard conventional hydration free energies of the H4C0, H3C1, H2C2, H1C3, FORM, ACET, and PROP ions; the H0C4 ion; and the IMID and GUAN ions, respectively, to be used in eq 3 for accessing the corresponding intrinsic values. These data are summarized in Table 2 .

II.1.2. Ammonium Ion; Mono-, Di-, Trimethyl-Ammonium Ions; Formate; Acetate; and Propanoate Ions. Kelly et al.[32] provide a compilation of absolute intrinsic hydration free energies for alkali and halide ions, as well as many other ions including polyatomic ones, based on experiments for the solvation of these ions in small gas-phase water clusters (containing 1−6 water molecules), and subsequent analysis of the experimental data relying on the cluster-pair correlation approach.[4,32,52] These hydration free energies are reported according to a convention of identical reference concentrations for the gas and aqueous phases, i.e., correspond to point-to-point parameters, and are anchored to an absolute intrinsic point-to-point proton hydration free energy of[32−34] $\Delta G^{\boxminus,\mathrm{alt}}_{\mathrm{hyd}}[\mathrm{H}^+_{\mathrm{g}}] = -1112.5$ kJ·mol^{-1}, corresponding to $\Delta G^{\ominus,\mathrm{alt}}_{\mathrm{hyd}}[\mathrm{H}^+_{\mathrm{g}}] = -1104.5$ kJ·mol^{-1} *via* eq 4. The superscript "alt" indicates here values that differ from those retained in the present parametrization work, namely $\Delta G^{\boxminus}_{\mathrm{hyd}}[\mathrm{H}^+_{\mathrm{g}}] = -1107.95$ kJ·mol^{-1} and $\Delta G^{\ominus}_{\mathrm{hyd}}[\mathrm{H}^+_{\mathrm{g}}] = -1100$ kJ·mol^{-1}.

Here, conventional hydration free energies $\Delta G^{\bullet}_{\mathrm{hyd}}[\mathrm{I}^z_{\mathrm{g}}]$ for the ions H4C0, H3C1, H2C2, H1C3, FORM, ACET, and PROP were deduced from the single-ion intrinsic point-to-point hydration free energies $\Delta G^{\boxminus,\mathrm{alt}}_{\mathrm{hyd}}[\mathrm{I}^z_{\mathrm{g}}]$ reported in ref 32 *via*

$$\Delta G^{\bullet}_{\mathrm{hyd}}[\mathrm{I}^z_{\mathrm{g}}] = \Delta G^{\boxminus,\mathrm{alt}}_{\mathrm{hyd}}[\mathrm{I}^z_{\mathrm{g}}] - z\Delta G^{\ominus,\mathrm{alt}}_{\mathrm{hyd}}[\mathrm{H}^+_{\mathrm{g}}] + \Delta G^{\ominus}_{\mathrm{std}} \quad (5)$$

which follows from eqs 3 and 4. Application of eq 3 with $\Delta G^{\ominus}_{\mathrm{hyd}}[\mathrm{H}^+_{\mathrm{g}}] = -1100$ kJ·mol^{-1} then leads to the standard absolute intrinsic hydration free energies $\Delta G^{\ominus}_{\mathrm{hyd}}[\mathrm{I}^z_{\mathrm{g}}]$ used as target data. The corresponding values of $\Delta G^{\boxminus,\mathrm{alt}}_{\mathrm{hyd}}[\mathrm{I}^z_{\mathrm{g}}]$, $\Delta G^{\bullet}_{\mathrm{hyd}}[\mathrm{I}^z_{\mathrm{g}}]$, and $\Delta G^{\ominus}_{\mathrm{hyd}}[\mathrm{I}^z_{\mathrm{g}}]$ are reported in Table 2

II.1.3. Tetramethyl-Ammonium Ion. Since Kelly et al.[32] do not provide a value for the H0C4 ion, different sources of experimental data were resorted to. The conventional hydration free energy of the H0C4 ion was obtained using the Gibbs equation:

$$\Delta G^{\bullet}_{\mathrm{hyd}}[\mathrm{I}^z_{\mathrm{g}}] = \Delta H^{\bullet}_{\mathrm{hyd}}[\mathrm{I}^z_{\mathrm{g}}] - T^{-}\Delta S^{\bullet}_{\mathrm{hyd}}[\mathrm{I}^z_{\mathrm{g}}] \quad (6)$$

based on experimental estimates for the conventional hydration enthalpy $\Delta H^{\bullet}_{\mathrm{hyd}}[\mathrm{I}^z_{\mathrm{g}}]$ and entropy $\Delta S^{\bullet}_{\mathrm{hyd}}[\mathrm{I}^z_{\mathrm{g}}]$, which were derived as follows.

First, the enthalpy of formation $\Delta_{\mathrm{f}}H^{(\ominus)}[\mathrm{I}^z_{\mathrm{g}}]$ of the gas-phase H0C4 ion reported by Nagano et al.[53] was corrected for the improper use of Boltzmann rather than Fermi−Dirac statistics for the standard state of the gas-phase electron according to[4,36]

$$\Delta_{\mathrm{f}}H^{\ominus}[\mathrm{I}^z_{\mathrm{g}}] = \Delta_{\mathrm{f}}H^{(\ominus)}[\mathrm{I}^z_{\mathrm{g}}] + z\Delta_{\mathrm{f}}H^{(\ominus)\to\ominus} \quad (7)$$

the correction term

$$\Delta_{\mathrm{f}}H^{(\ominus)\to\ominus} = \Delta_{\mathrm{h}}H^{\ominus}[\mathrm{e}^-_{\mathrm{g}}] - \Delta_{\mathrm{h}}H^{(\ominus)}[\mathrm{e}^-_{\mathrm{g}}] \quad (8)$$

representing the difference in the heat-up enthalpies of the gas-phase electron according to Fermi−Dirac ($\Delta_{\mathrm{h}}H^{\ominus}[\mathrm{e}^-_{\mathrm{g}}]$) and Boltzmann ($\Delta_{\mathrm{h}}H^{(\ominus)}[\mathrm{e}^-_{\mathrm{g}}]$) statistics, and evaluating to[4] −3.1 kJ·mol^{-1}. Combination with the enthalpy of formation $\Delta_{\mathrm{f}}H^{\ominus}[\mathrm{H}^+_{\mathrm{g}}]$ of the gas-phase proton ($\Delta_{\mathrm{f}}H^{\ominus}[\mathrm{H}^+_{\mathrm{g}}] = 1533.1$ kJ·mol^{-1} from ref 36) and the conventional enthalpy of formation $\Delta_{\mathrm{f}}H^{\bullet}[\mathrm{I}^z_{\mathrm{aq}}]$ of the aqueous H0C4 ion (also from Nagano et al.[53]) yields the conventional hydration enthalpy $\Delta H^{\bullet}_{\mathrm{hyd}}[\mathrm{I}^z_{\mathrm{g}}]$ of the H0C4 ion:

$$\Delta H^{\bullet}_{\mathrm{hyd}}[\mathrm{I}^z_{\mathrm{g}}] = \Delta_{\mathrm{f}}H^{\bullet}[\mathrm{I}^z_{\mathrm{aq}}] - \Delta_{\mathrm{f}}H^{\bullet}[\mathrm{I}^z_{\mathrm{g}}] \quad (9)$$

where, similar to eq 3,

$$\Delta_{\mathrm{f}}H^{\bullet}[\mathrm{I}^z_{\mathrm{g}}] = \Delta_{\mathrm{f}}H^{\ominus}[\mathrm{I}^z_{\mathrm{g}}] - z\Delta_{\mathrm{f}}H^{\ominus}[\mathrm{H}^+_{\mathrm{g}}] \quad (10)$$

Note that the resulting value $\Delta H^{\bullet}_{\mathrm{hyd}}[\mathrm{I}^z_{\mathrm{g}}] = 885.0$ kJ·mol^{-1} is identical to the one that can be deduced from the estimated standard absolute intrinsic hydration enthalpies of the proton and of the H0C4 ion as reported by Marcus,[54] which represents a useful consistency check.

Second, the conventional hydration entropy of the H0C4 ion was deduced from the conventional partial molar entropy of the aqueous H0C4 ion, as

$$s^{\bullet}[\mathrm{I}^z_{\mathrm{aq}}] = s^{\ominus,\mathrm{alt}}[\mathrm{I}^z_{\mathrm{aq}}] - zs^{\ominus,\mathrm{alt}}[\mathrm{H}^+_{\mathrm{aq}}] \quad (11)$$

using data for $s^{\ominus,\mathrm{alt}}[\mathrm{I}^z_{\mathrm{aq}}]$ and $s^{\ominus,\mathrm{alt}}[\mathrm{H}^+_{\mathrm{aq}}]$ reported by Marcus.[54] Combination with the absolute molar entropy $s^{\ominus}[\mathrm{H}^+_{\mathrm{g}}]$ of the gas-phase proton ($s^{\ominus}[\mathrm{H}^+_{\mathrm{g}}] = 108.95$ J·mol^{-1}·K^{-1} from ref 36) and the corresponding value $s^{\ominus}[\mathrm{I}^z_{\mathrm{g}}]$ for the gaseous H0C4 ion (also from Marcus[54,55]) yields the conventional hydration entropy $\Delta S^{\bullet}_{\mathrm{hyd}}[\mathrm{I}^z_{\mathrm{g}}]$ of the H0C4 ion:

$$\Delta S^{\bullet}_{\mathrm{hyd}}[\mathrm{I}^z_{\mathrm{g}}] = s^{\bullet}[\mathrm{I}^z_{\mathrm{aq}}] - s^{\bullet}[\mathrm{I}^z_{\mathrm{g}}] \quad (12)$$

where, similar to eq 3,

$$s^{\bullet}[\mathrm{I}^z_{\mathrm{g}}] = s^{\ominus}[\mathrm{I}^z_{\mathrm{g}}] - zs^{\ominus}[\mathrm{H}^+_{\mathrm{g}}] \quad (13)$$

The conventional hydration free energy of the H0C4 ion is obtained from eq 6. Application of eq 3 with $\Delta G^{\ominus}_{\mathrm{hyd}}[\mathrm{H}^+_{\mathrm{g}}] = -1100$ kJ·mol^{-1} then leads to the standard absolute intrinsic hydration free energy $\Delta G^{\ominus}_{\mathrm{hyd}}[\mathrm{I}^z_{\mathrm{g}}]$ used as target data. The values of all of the quantities involved in this calculation, as well as the resulting estimate for $\Delta G^{\ominus}_{\mathrm{hyd}}[\mathrm{I}^z_{\mathrm{g}}]$, are reported in Table 2.

II.1.4. Imidazolium and Guanidinium Ions. Since neither gas-phase nor aqueous-phase formation data could be found for the IMID and GUAN ions, a different approach was chosen here to obtain conventional hydration free energies. A thermodynamic cycle (Figure 1) consisting of gas-phase and aqueous-phase deprotonation reactions involving the positively

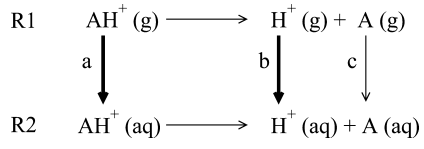

Figure 1. Thermodynamic cycle connecting the free energies of the deprotonation reactions (horizontal legs R_1 and R_2) of the ionic species AH^+_g and AH^+_{aq} in the gas phase and the aqueous phase, respectively, to the hydration free energies (vertical legs a, b, and c) of the ionic (AH^+_g) and neutral (A_g) species, as well as of the proton (H^+_g). This cycle allows for a calculation of the conventional hydration free energy of the ionic species, $\Delta G^{\bullet}_{\mathrm{hyd}}[\mathrm{AH}^+_{\mathrm{g}}]$, through eq 14, which requires knowledge of the gas phase basicity GB of A_g (i.e., the free-energy change of reaction R1; $\Delta G^{\ominus}_{\mathrm{R1}} = \mathrm{GB}$), of the p$K_a$ of AH^+_{aq} in water (related to the free-energy change of reaction R2; $\Delta G^{\ominus}_{\mathrm{R2}} = RT^{-}\mathrm{p}K_a \ln 10$), and of the standard hydration free energy of the neutral compound, $\Delta G^{\ominus}_{\mathrm{hyd}}[\mathrm{A}_{\mathrm{g}}]$ (i.e., the free-energy change along leg c). The conventional hydration free energy $\Delta G^{\bullet}_{\mathrm{hyd}}[\mathrm{AH}^+_{\mathrm{g}}]$ is given by the difference between the free-energy changes associated with legs a and b, $\Delta G^{\bullet}_{\mathrm{hyd}}[\mathrm{AH}^+_{\mathrm{g}}] = \Delta G^{\ominus}_{\mathrm{hyd}}[\mathrm{AH}^+_{\mathrm{g}}] - \Delta G^{\ominus}_{\mathrm{hyd}}[\mathrm{H}^+_{\mathrm{g}}]$(eq 3 with $z = 1$).

dx.doi.org/10.1021/ct300156h | J. Chem. Theory Comput. 2012, 8, 3705−3723

charged (AH_g^+, AH_{aq}^+) and neutral (A_g, A_{aq}) IMID and GUAN species was constructed. The free-energy change ΔG_{R1} associated with the gas-phase deprotonation reaction (R1) is given by the gas phase basicities, GB (corresponding to an ideal-gas reference pressure of 1 bar), of the imidazole and guanidine molecules. Following the usual convention,[56] the gas-phase basicity refers here to the negative of the proton-capture free energy, i.e., actually corresponds to a proton dissociation (acidity) parameter. The free-energy change ΔG_{R2} associated with the aqueous-phase deprotonation reaction (R2) is given by the acidity constants K_a (corresponding to an ideal-solution reference concentration of 1 m) of the imidazolium and guanidinium species. The conventional hydration free energies of the protonated species can thus be deduced as (Figure 1)

$$\begin{aligned}\Delta G_{hyd}^{\bullet}[AH_g^+] &= \Delta G_{hyd}^{\ominus}[AH_g^+] - \Delta G_{hyd}^{\ominus}[H_g^+] \\ &= \Delta G_{R1}^{\ominus} - \Delta G_{R2}^{\ominus} + \Delta G_{hyd}^{\ominus}[A_g] \\ &= \mathrm{GB} - RT^- \mathrm{p}K_a \ln 10 + \Delta G_{hyd}^{\ominus}[A_g]\end{aligned} \tag{14}$$

where pK_a is the negative decadic logarithm of the acidity constant K_a and $\Delta G_{hyd}^{\ominus}[A_g]$ is the standard hydration free energy of the neutral species. Using tabulated data for gas-phase basicities[57] and pK_a values,[58] estimates for $\Delta G_{hyd}^{\bullet}[AH_g^+]$ can thus be obtained, provided that a corresponding value for $\Delta G_{hyd}^{\ominus}[A_g]$ is available (see below). The resulting conventional hydration free energies are expected to present a higher uncertainty than conventional hydration free energies obtained from the approaches outlined in sections II.1.2 and II.1.3, because gas-phase basicities have estimated errors of up to[56,59] 8 kJ·mol^{-1}. Application of eq 3 with $\Delta G_{hyd}^{\ominus}[H_g^+] = -1100$ kJ·mol^{-1} then leads to the standard absolute intrinsic hydration free energy $\Delta G_{hyd}^{\ominus}[I_g^z]$ used as target data. The values of all of the quantities involved in this calculation, as well as the resulting estimate for $\Delta G_{hyd}^{\ominus}[AH_g^+]$ are reported in Table 2.

In the case of the IMID ion, the experimental value of $\Delta G_{hyd}^{\ominus}[A_g]$ is taken from ref 60 (after standard-state conversion). In the case of the GUAN ion, a complication arises because the hydration free energy of the guanidine molecule is not available. This value is approximated here based on the corresponding value for the methyl-guanidine molecule, available experimentally in ref 60, decreased by 1.3 kJ·mol^{-1}. This approximate adjustment is inferred from the hydration free energies of a series of small polar organic molecules[61] differing by the presence or absence of one methyl group. The precise value chosen for this hydration free energy increment of the methyl group does not play a significant role, considering that the simulation results are affected by statistical errors of the same order of magnitude (1−2 kJ·mol^{-1}).

The relatively high uncertainty associated with conventional hydration free energy estimates based on the deprotonation-cycle approach (Figure 1) might seem discomforting at first sight. However, application of the same procedure (eq 14) to the H3C1 and ACET ions using gas phase basicities[57] of 864.5 and 1428.7 kJ·mol^{-1}, respectively (the latter being an arithmetic average of three reported values[57] 1427, 1429, and 1430 kJ·mol^{-1}) and pK_a values[62] of 10.6 and 4.8, respectively, in conjunction with standard hydration free energies for the neutral species[60] of −11.2 and −20.1 kJ·mol^{-1}, respectively (converted from the corresponding point-to-point values reported in ref 60 according to eq 4), yields $\Delta G_{hyd}^{\bullet}[I_g^z]$ estimates of −307.3 and −321.4 kJ·mol^{-1}, in remarkably good agreement with the values obtained in section II.1.2, as reported in Table 2.

II.2. Molecular Dynamics Simulations. All MD simulations were performed either with a modified version of the GROMOS96 program[6,63] or with the GROMOS11 program.[64] The former was exclusively used for free-energy calculations in simulations employing the particle−particle−particle−mesh (P^3M) method[65,66] for the treatment of electrostatic interactions. The ions were described using either the 54A7 or the 54A8 (present work; section II.4) parameter sets, and water was represented by means of the three-site SPC model.[17] The present section provides generic information concerning the simulation procedures employed in this work. Additional details specific to the determination of single-ion hydration free energies, of reoptimized force-field parameters, of ion−solvent RDFs, and of ion−ion PMFs are provided in sections II.3−II.6, respectively.

All simulations were carried out under periodic boundary conditions (PBC) based on cubic computational boxes. The equations of motion were integrated using the leapfrog scheme[67] with a time step of 2 fs. The solute bond-length distances and the rigidity of the water molecules were enforced by application of the SHAKE algorithm[68] with a relative geometric tolerance of 10^{-4}. The center of mass translation of the computational box was removed every 2 ps. The temperature was maintained at $T^- = 298.15$ K by weak coupling to a heat bath[69] using a coupling time of 0.1 ps. The pressure was maintained at $P^\circ = 1$ bar by weak coupling to a pressure bath with isotropic coordinate scaling,[69] using a value of 45.2×10^{-6} bar^{-1} = 7.513×10^{-4} (kJ·mol^{-1}·nm^{-3})$^{-1}$ for the isothermal compressibility of water[70] and a coupling time of 0.5 ps. Two different electrostatic schemes were employed during the simulations:[26,38] (*i*) cutoff-truncated (CT) electrostatic interactions with a Barker−Watts reaction-field correction[18] and a molecule-based cutoff (BM) and (*ii*) particle−particle−particle−mesh (P^3M) electrostatic interactions with tinfoil boundary conditions, i.e., a lattice-sum (LS) method.

The BM scheme was applied with a value $\varepsilon_{BW} = 66.6$ for the relative permittivity of the dielectric continuum surrounding the cutoff sphere, as appropriate[71] for the SPC water model. The RF self-energy term[72,73] was included in the calculation of the energy, but not of the electric potential at the ion sites, considering that the correction scheme for single-ion solvation free energies[26,38] is designed for raw results excluding this contribution. This term induces no virial (pressure) contribution. In all BM simulations, the long-range interactions were truncated at a charge-group cutoff distance $R_C = 1.4$ nm and calculated at each time step based on a pairlist that was updated at each time step.

The LS scheme was applied with[74] a spherical hat charge-shaping function of width 1.0 nm, a triangular shaped cloud assignment function, a finite-difference scheme of order 2, and a grid-spacing of about 0.1 nm. This choice of parameters led to a ratio of the root-mean square error in the atomic forces to the average norm of these forces[66,75,76] of about 0.5%. The self-energy term[66,73,77−79] was included in the calculation of the energy and of the virial (pressure), but not of the electric potential at the ion sites, considering that the correction scheme for single-ion solvation free energies[26,38] is designed for raw results excluding this contribution. Because its effect was found to be negligible in a previous study of ion solvation free energies,[25] the self-energy contribution to the virial[80] was not removed here. In all LS simulations, the Lennard-Jones

interactions were truncated at an atom-based cutoff-distance R_C = 1.0 nm. Both real-space electrostatic and Lennard-Jones interactions were calculated at each time step based on a pairlist updated at each time step.

For the calculations of single-ion hydration free energies (section II.3), both the BM and LS schemes were employed. The MD simulations involved cubic computational boxes containing one ion (charge state q_I') and N_w = 512 or 1024 water molecules. The calculation of a hydration free energy was performed in two thermodynamic-integration procedures,[81] considering separately the work of creating a neutral ion-sized cavity (cavitation free energy ΔG_{cav}) and of charging this cavity (raw charging free energy ΔG_{chg}^{raw}). All production simulations (different ions, ionic charge states or cavity-size scaling factors, and electrostatic interaction schemes) for the free-energy calculations were preceded by an equilibration period of 0.2 ns and lasted 1 ns (charging) or 0.4 ns (cavitation). The configurations sampled along these simulations were written to file every 0.1 ps (full ionic charge state only) or 0.3 ps for subsequent analysis, while the corresponding energetic data were written every 0.1 ps.

The calculation of the ion−solvent RDFs (section II.5) relied on the subset of the above simulations performed using the BM scheme at the full cavity size and ionic charge state. The calculations of ion−ion PMFs (section II.6) relied on umbrella sampling.[82,83] Here also, only the BM scheme was considered. The MD simulations involved cubic computational boxes containing one ion pair and 2139−2143, 2134−2138, 2138−2142, 2136−2138, 2140−2143, 2139−2143, 2140−2143, or 2141−2144 water molecules in the N_u umbrella-sampling windows for the ACET-NA, ACET-GUAN, ACET-H3C1, ACET-IMID, GUAN-CL, H3C1-CL, IMID-CL, and NA-CL systems, respectively. The slightly different numbers of water molecules in the different windows arise because for each window, the initial configuration was constructed by solvating the ion pair in a cubic computational box of 4.0 nm edge length containing equilibrated solvent molecules, respecting a minimum ion−solvent distance of 0.23 nm. The degrees of freedom of the two ionic species and of the solvent molecules were coupled to separate temperature baths, except for the NA-CL system, where the NA and CL ions (only six degrees of freedom) were coupled to the same temperature bath as the solvent. For each window, the simulations were preceded by an equilibration period of 0.1 ns, and lasted 1.2 ns. The configurations sampled along these simulations were written to file every 0.3 ps for subsequent analysis.

II.3. Free-Energy Calculations. *II.3.1. Thermodynamic Cycle.* The standard solvation free energy of a species corresponds to the reversible work of transferring this species from the ideal gas phase to the ideal solution environment, given appropriate standard-state definitions for the two phases. In terms of the corresponding point-to-point quantity, this is equivalent to the transfer of a single molecule of the species from a fixed position in vacuum to a fixed position in the bulk solvent. Computationally, however, simulating the transfer of a species across a phase interface is rather challenging. For this reason, a thermodynamic cycle is considered instead, where the molecule is annihilated in vacuum, transferred to the solution, and recreated in the solution environment. The Hamiltonian of the annihilated state of the molecule is selected in such a way that it excludes any solute−solvent interactions. As a result, the transfer of the molecule from the vacuum to the solution environment in this state is associated with a zero free-energy change. For simplicity, the covalent interactions and atomic masses are kept unaltered in the annihilated state. This ensures that the kinetic energy provides no contribution to the free-energy derivative along the process. As a result, the condition of fixed position of the molecule in vacuum or in solution can be relaxed in the calculation without altering its outcome.

Within these conditions, the annihilated state can be selected in different ways. The most common choice is to zero the partial charges and Lennard-Jones interaction parameters of all atoms in the molecule, leaving a skeleton of covalently bound "dummy" atoms exempt of any nonbonded (intra- and intermolecular) interactions. The solvation free energy is then calculated as

$$\Delta G_{slv} = \Delta G_{crea}^{sol} - \Delta G_{crea}^{vac} \tag{15}$$

where

$$\Delta G_{crea}^{sol} = \int d\lambda \left\langle \frac{\partial [U^{intra}(\mathbf{x};\lambda) + U^{inter}(\mathbf{x};\lambda)]}{\partial \lambda} \right\rangle_{\lambda,sol} \tag{16}$$

and

$$\Delta G_{crea}^{vac} = \int d\lambda \left\langle \frac{\partial U^{intra}(\mathbf{x}_p;\lambda)}{\partial \lambda} \right\rangle_{\lambda,vac} \tag{17}$$

i.e., the creation of the molecule in solution (eq 16) is associated with the progressive installation of λ-dependent intra- and intermolecular interactions $U^{intra}(\mathbf{x};\lambda)$ and $U^{inter}(\mathbf{x};\lambda)$, respectively, while its creation in vacuum (eq 17) is associated with the progressive installation of λ-dependent intramolecular interactions $U^{intra}(\mathbf{x}_p;\lambda)$ only, $\mathbf{x} = \{\mathbf{x}_p,\mathbf{x}_s\}$ denoting the $3N$-dimensional coordinate vector of the system containing N_p solute atoms and N_s solvent atoms, λ denoting the scaling parameter of the thermodynamic integration procedure,[81] and $\langle ... \rangle_{\lambda,sol}$ and $\langle ... \rangle_{\lambda,vac}$ denoting ensemble averaging over configurations sampled during simulations in solution (system coordinate vector $\mathbf{x}$) and in vacuum (system coordinate vector $\mathbf{x}_p$), respectively. In the present work, the solvation free energy is calculated as

$$\begin{aligned} \Delta G_{slv} &= \Delta G_{crea}^{sol} - \Delta G_{crea}^{vac} \\ &\approx \int d\lambda \left\langle \frac{\partial U^{inter}(\mathbf{x};\lambda)}{\partial \lambda} \right\rangle_{\lambda,sol} \end{aligned} \tag{18}$$

where eqs 16 and 17 were used, and it was assumed that the free-energy contribution associated with the installation of intramolecular nonbonded interactions is identical in vacuum and in solution, i.e.

$$\int d\lambda \left\langle \frac{\partial U^{intra}(\mathbf{x};\lambda)}{\partial \lambda} \right\rangle_{\lambda,sol} \approx \int d\lambda \left\langle \frac{\partial U^{intra}(\mathbf{x}_p;\lambda)}{\partial \lambda} \right\rangle_{\lambda,vac} \tag{19}$$

the error introduced by this approximation being essentially negligible for rigid solute species. Since the ions considered in this study are essentially rigid, with the possible exception of PROP, this approximation is expected to affect the results only marginally. For PROP, the same statement almost certainly holds, considering that the mobile methyl group is exempt of atomic partial charge.

The electrostatic component $U_{elec}^{inter}(\mathbf{x};\lambda)$ of the λ-dependent part of the intermolecular energy $U^{inter}(\mathbf{x};\lambda)$ in eq 18 was calculated on the basis of the sampled configurations as

$$U_{elec}^{inter}(\mathbf{x};\lambda) = (4\pi\varepsilon_o)^{-1}\lambda\{\sum_{i=1}^{N_p}\sum_{j>i}^{N_p} q_i q_j[\psi_{ij}(\mathbf{x}_p) - r_{ij}^{-1}(\mathbf{x}_p)] + \sum_{i=1}^{N_p}\sum_{j=1}^{N_s} q_i q_j \psi_{ij}(\mathbf{x})\} \quad (20)$$

where q_i is the partial charge of atom i, $r_{ij}(\mathbf{x}_p)$ is the interatomic distance, and $\psi_{ij}(\mathbf{x})$ is the effective pairwise electrostatic interaction function according to a modified GROMOS Hamiltonian exempt of self-energy term (manuscript in preparation). The sampling of configurations was performed according to an unmodified GROMOS Hamiltonian in the NPT ensemble (section II.2); i.e., it included a configuration-independent self-energy term which induces a nonvanishing self-virial contribution in the LS scheme (self-energy term dependent on box-edge length) and a vanishing self-virial contribution in the BM scheme (self-energy term independent of box-edge length).[64] Omission of a possible correction[80] to the LS self-virial for the presence of a nonzero net charge is expected to result in a negligible error for the systems considered in the present study.[25]

II.3.2. Raw Hydration Free Energy. The standard hydration free energy $\Delta G_{hyd}^{\ominus}$ of an ion is calculated as the sum of the charging free energy ΔG_{chg}, the cavitation free energy ΔG_{cav}, and the standard-state conversion term $\Delta G_{std}^{\ominus}$ (eq 4), i.e., as

$$\Delta G_{hyd}^{\ominus} = \Delta G_{chg} + \Delta G_{cav} + \Delta G_{std}^{\ominus} \quad (21)$$

where ΔG_{chg} consists of a methodology-dependent raw charging free energy ΔG_{chg}^{raw} and a correction contribution ΔG_{cor}, the evaluation of the latter being explained in section II.3.3.

The raw charging free energies ΔG_{chg}^{raw} were calculated for the different ions using the BM or LS electrostatic schemes (section II.2) by reversibly charging the ion according to the thermodynamic-integration approach[81] (trapezoidal rule), which requires the evaluation of the average of the solvent-generated electric potential at the atomic sites of the ion for different ionic charge states q_I' from zero to full ionic charge q_I. Eleven charge states (q_I'/q_I = 0.0, 0.1, ..., 0.9, 1.0) were used for all ions. This is sufficient considering that the resulting curves for the average potential are almost linear. For each charge state q_I', the charges q_i of the atoms i of the ion were scaled in the same fashion, i.e., $q_i'/q_i = q_I'/q_I \; \forall \; i$, where q_i' denotes the partial charge of atom i at charge state q_I'. The electric potential evaluated at the different atomic sites of the ion was exempt of intramolecular contributions, as detailed in section II.3.1.

Cavitation free energies ΔG_{cav} were also calculated for the different ions by thermodynamic integration[81] (trapezoidal rule) over the ensemble average of the derivative of the Hamiltonian with respect to a scaling parameter λ applied to the ion−water Lennard-Jones interactions at zero charge (q_I' = 0), from no interaction at $\lambda = 0$ to full interaction at $\lambda = 1$, using a soft-core potential[6,84] with $\alpha_{LJ} = 0.5$ and based on at least 21 intermediate growth states. Because ΔG_{cav} is of small magnitude compared to ΔG_{chg}^{raw} and only weakly affected by methodology-dependent errors,[25,26] this calculation was only performed for one system size (N_w = 1024) and one electrostatic interaction scheme (BM scheme). Here also, the derivative of the Hamiltonian with respect to λ was exempt of intramolecular contributions, as explained in section II.3.1.

Throughout, statistical error estimates on ensemble averages pertaining to particular q_I' or λ values were obtained from block averaging.[1] The error on the free-energy value was calculated by numerical integration of the individual errors.

II.3.3. Free-Energy Correction Terms. The raw charging free energies ΔG_{chg}^{raw} (section II.3.2) were used to calculate corresponding methodology-independent values ΔG_{chg} as[25,26,38]

$$\Delta G_{chg} = \Delta G_{chg}^{raw} + \Delta G_{cor} \quad (22)$$

where ΔG_{cor} is a free-energy correction for the various methodology-dependent errors committed during the simulation, namely (see refs 4, 25, 26 and references therein):

(A) The deviation of the solvent polarization around the ion relative to the polarization in an ideal Coulombic system and the incomplete interaction of the ion with the polarized solvent, a consequence of possible approximations made in the representation of electrostatic interactions during the simulation (e.g., non-Coulombic interactions involving cutoff truncation and, possibly, a reaction-field correction). This type-A correction is evaluated for the given approximate electrostatic scheme used in the simulation (e.g., BM scheme), but in the idealized context of a macroscopic system. For CT schemes, it can be subdivided into a type-A_1 correction, acting beyond the cutoff sphere of the ion, and a type-A_2 correction, acting within this sphere. There is no such correction for LS schemes, which are Coulombic in the limit of infinite system (box) sizes.

(B) The deviation of the solvent polarization around the ion relative to the polarization in an ideal macroscopic system, a consequence of the use of a finite (microscopic) system during the simulation (e.g., computational box simulated under PBC). This type-B correction is evaluated for the given approximate electrostatic scheme used in the simulation.

(C) The deviation of the solvent-generated electric potential at the atomic sites of the ion as calculated from the simulated trajectory relative to the "correct" electric potential, a consequence of the possible application of an inappropriate summation scheme (along with a possibly non-Coulombic potential function) for the contributions of individual solvent atomic charges to this potential (i.e., P scheme, summing over individual charges, vs M scheme, summing over charges within individual solvent molecules), as well as of the possible presence of a constant offset in this potential (e.g., due to the presence of an interfacial potential at the surface of the ion along with the constraint of vanishing average potential in the LS scheme). This type-C correction is evaluated for the given approximate electrostatic scheme and choice of boundary conditions used in the simulation and can be subdivided into a type-C_1 correction for improper potential summation and a type-C_2 correction for the potential offset.

(D) An inaccurate dielectric permittivity of the employed solvent model.

The application of this correction scheme to the solvation of monatomic ions has been illustrated in several recent studies.[25,26,38] Its extension to polyatomic ions requires a

numerical solution of the Poisson equation to obtain a continuum-electrostatics estimate for the charging free energy of the ionic solute in a macroscopic nonperiodic system with Coulombic electrostatic interactions and based on the experimental solvent permittivity, ΔG_{chg}^{NPBC}, and in a periodic system with a specific electrostatic interaction scheme and based on the model solvent permittivity, e.g., $\Delta G_{chg}^{PBC,BM}$ for the BM scheme or $\Delta G_{chg}^{PBC,LS}$ for the LS scheme. The sum of the type-A, -B, and -D corrections introduced above can be deduced from the results of these two continuum-electrostatics calculations, as

$$\Delta G_{A+B+D}^{LS} = \Delta G_{chg}^{NPBC} - \Delta G_{chg}^{PBC,LS} \tag{23}$$

for the LS scheme and

$$\Delta G_{A+B+D}^{BM} = \Delta G_{chg}^{NPBC} - \Delta G_{chg}^{PBC,BM} \tag{24}$$

for the BM scheme. Here, the relative dielectric permittivity is set to 78.4 in the calculation of ΔG_{chg}^{NPBC}, as appropriate for water,[4] and to 66.6 in the calculations of $\Delta G_{chg}^{PBC,LS}$ and $\Delta G_{chg}^{PBC,BM}$, as appropriate for the SPC water model.[71]

In practice, eq 23 is evaluated numerically as

$$\Delta G_{A+B+D}^{LS} = \Delta G_{chg}^{NPBC,FD} - \Delta G_{chg}^{PBC,LS,FD} \tag{25}$$

where $\Delta G_{chg}^{NPBC,FD}$ and $\Delta G_{chg}^{PBC,LS,FD}$ are charging free energies evaluated with the finite-difference (FD) Poisson equation solver of refs 85−87 employing Coulombic electrostatic interactions under nonperiodic and periodic boundary conditions, respectively. Analogously, eq 24 is evaluated numerically as

$$\Delta G_{A+B+D}^{BM} = \Delta G_{chg}^{NPBC,FD} - \Delta G_{chg}^{PBC,LS,FD} + \Delta G_{chg}^{PBC,LS,FFT} - \Delta G_{chg}^{PBC,BM,FFT} \tag{26}$$

where $\Delta G_{chg}^{PBC,LS,FFT}$ and $\Delta G_{chg}^{PBC,BM,FFT}$ are charging free energies evaluated with the fast Fourier transform (FFT) Poisson equation solver of refs 88 and 89 considering LS and BM interactions, respectively, under periodic boundary conditions. The application of two LS calculations (subtraction and addition of the terms $\Delta G_{chg}^{PBC,LS,FD}$ and $\Delta G_{chg}^{PBC,LS,FFT}$, respectively) enhances the cancellation of grid-discretization and boundary-smoothing errors in the two different algorithms.

Since the ions considered in this study are essentially rigid, with the possible exception of PROP, the calculation of ΔG_{A+B+D} was only performed on the basis of a single structure, taken as the final solute configuration of the LS simulation at full cavity size and ionic charge state in the system involving N_w = 1024 water molecules (section II.2). For PROP, this structure presents C−C−C−O dihedral angle values of about 90°, very close to the corresponding simulation averages. The different terms of eqs 25 and 26 were evaluated using the appropriate Poisson equation solver, boundary conditions, electrostatic scheme, and solvent permittivity, based on a grid spacing of about 0.02 nm and a threshold of 10^{-6} kJ·mol^{-1} for the convergence of the electrostatic free energy. A van der Waals envelope was used to define the solute low-dielectric cavity, where the atomic radii were based on distances at the minimum of the Lennard-Jones potential between the different solute atoms and the oxygen atom of a SPC water molecule[17] using the Lennard-Jones interaction parameters of either the 54A7 or the 54A8 parameter sets, reduced by an estimate[90] for the radius of a water molecule (0.14 nm). Polar hydrogen atoms were treated differently[91,92] and assigned an atomic radius of 0.05 nm.

The term ΔG_{C_1} corrects for the P-summation scheme implied by the LS and BM schemes, relative to a proper M-summation scheme. This correction term was derived previously for a monatomic (spherical) ion.[37] It is easily seen that the solvent contribution to this term is unaltered when the ion is polyatomic and the ionic cavity nonspherical, provided that one evaluates it on the basis of the total ionic charge (q_I). In this case, one has[25,26,37]

$$\Delta G_{C_1}^{LS} = -N_A q_I \left(1 - \frac{V_I}{\langle L \rangle^3}\right) \xi_S' \tag{27}$$

for the LS scheme and

$$\Delta G_{C_1}^{BM} = -N_A q_I \frac{2(\varepsilon_{BW} - 1)}{2\varepsilon_{BW} + 1} \left(1 - \frac{V_I}{(4/3)\pi R_C^3}\right) \xi_S' \tag{28}$$

for the BM scheme, where N_A is Avogadro's constant, V_I is the ionic volume (assumed constant throughout the simulation), ε_{BW} is the reaction-field permittivity, R_C is the cutoff distance, and ξ'_S is the exclusion potential[37] of the solvent model. For fully rigid models with a single van der Waals interaction site, it is easily shown that the exclusion potential is given by[4,93]

$$\xi_S' = (6\varepsilon_o)^{-1} \eta_w \gamma_w \tag{29}$$

where γ_w is the quadrupole moment trace of the solvent model relative to its single van der Waals interaction site, which is readily calculated from the knowledge of its geometry and charge distribution, and η_w is the solvent number density. For the SPC water model,[17,37] γ_w = 0.0082e·nm^2, and η_w was evaluated in the present study as

$$\eta_w = \frac{N_w}{\langle L \rangle^3 - V_I} \tag{30}$$

Note that eq 30 differs from the expression $\eta_w = (N_w + 1)\langle L \rangle^{-3}$ used in previous work on monatomic ions,[25,26,38] where V_I was approximated by the volume of a water molecule. Inserting eqs 29 and 30, eqs 27 and 28 become

$$\Delta G_{C_1}^{LS} = -N_A (6\varepsilon_o)^{-1} N_w \gamma_w q_I \frac{1}{\langle L \rangle^3} \tag{31}$$

and

$$\Delta G_{C_1}^{BM} = -N_A (6\varepsilon_o)^{-1} \frac{2(\varepsilon_{BW} - 1)}{2\varepsilon_{BW} + 1} N_w \gamma_w q_I \frac{1 - [(4/3)\pi R_C^3]^{-1} V_I}{\langle L \rangle^3 - V_I} \tag{32}$$

respectively. For the LS scheme, $\Delta G_{C_1}^{LS}$ turns out to be independent of V_I. This is not the case in the BM scheme, and different choices for V_I were tested, namely, (*i*) the change in the volume of the computational box upon insertion of the neutral ion-sized cavity; (*ii*) the change in the volume of the computational box upon insertion of the fully charged ion; (*iii*) a sum of atomic volumes (using the atomic radius definition described above, as well as an alternative definition employing Lennard-Jones collision diameters rather than minima), with atomic radii scaled by factors 0.7, 0.8, 0.9, or 1.0 (to correct for the overlap of individual atomic volumes). These volumes and the resulting $\Delta G_{C_1}^{BM}$ values are reported and discussed in the Supporting Information. The first volume definition was ultimately retained for all calculations, considering that it is

essentially independent of the simulation methodology, physically meaningful, and exempt of the choice of an arbitrary scaling factor. Note, however, that the values of $\Delta G_{C_1}^{BM}$ calculated using the nine above alternative definitions differ by at most 1.4 kJ·mol^{-1}, indicating that this choice has little impact on the final results. In fact, eq 32 could even be approximated as

$$\Delta G_{C_1}^{BM} \approx \Delta G_{C_1}^{LS} \tag{33}$$

with a limited loss of accuracy, i.e., at most 2.5 kJ·mol^{-1} error considering the present calculations with $N_w = 1024$.

In the case of a monatomic ion, eqs 31 and 32 represent the only contributions to the type-C_1 correction term, because a monatomic ion has a vanishing quadrupole moment trace relative to its single van der Waals interaction site. In the case of a polyatomic ion, however, they only represent the solvent contribution to this term and omit a possible additional contribution related to the quadrupole-moment trace of the ion itself. The form of this term is discussed in Supporting Information. Because the magnitude of the corresponding contribution is very small in the context of the present calculations, this term was neglected in ΔG_{cor}.

Finally, under PBC, the term ΔG_{C_2} corrects for the presence of an interfacial potential at the ion surface. For a monatomic ion, this term is given by[38] (note that eq 33 of ref 38 incorrectly includes an additional term ΔG_B^{LS}):

$$\Delta G_{C_2}^{LS} = (N_A q_I \Phi_0^{raw} + \Delta G_{C_1}^{LS}) \frac{V_I}{\langle L \rangle^3} \tag{34}$$

where Φ_0^{raw} is the raw electric potential in the neutral ion-sized cavity. However, because this term is proportional to the ratio of the ionic volume to the box volume, its magnitude is very small for the systems considered here. For this reason, and because its generalization to polyatomic ions is not straightforward, this term was also neglected in the calculation of ΔG_{cor}.

Given the above correction terms, the standard hydration free energy $\Delta G_{hyd}^{\ominus}$ is calculated according to eqs 21 and 22 as the sum of the raw charging free energy ΔG_{chg}^{raw}, the cavitation free energy ΔG_{cav}, and the standard-state conversion term $\Delta G_{std}^{\ominus}$, along with the correction terms ΔG_{A+B+D} (eqs 25 and 26) and ΔG_{C_1} (eqs 31 and 32), as

$$\Delta G_{hyd}^{\ominus} = \Delta G_{chg}^{raw} + \Delta G_{A+B+D} + \Delta G_{C_1} + \Delta G_{cav} + \Delta G_{std}^{\ominus} \tag{35}$$

These standard hydration free energies were calculated for the 10 ions considered, based on either the 54A7 or the 54A8 parameter sets, and can be compared to the corresponding experimental estimates (section II.1).

II.4. Reoptimization of the Force-Field Parameters. On the basis of the hydration free energies calculated for the 10 ions using the 54A7 force field, a reoptimization of the parameters was performed so as to improve the agreement with experimental data, leading to the refined 54A8 parameter set. The calibration focused in the first place on the ions H4C0, H3C1, H0C4, ACET, IMID, and GUAN and was guided by the following principles: (*i*) the covalent interaction parameters were kept unaltered relative to 54A7; (*ii*) the Lennard-Jones interaction parameters were also kept unaltered, except for the five ammonium ions (see below); (*iii*) the charge-group definitions were also kept unaltered, except for the three carboxylate ions and the IMID ion (see below). The optimization thus concerned nearly exclusively the atomic partial charges. Since these represent 3−5 free parameters for the different ions, to be calibrated against a single observable in each case, this optimization involves a certain extent of arbitrariness, and some choices had to be made based on comparison with the 54A7 force field and chemical intuition. In the case of the five ammonium ions, the Lennard-Jones interaction parameters of the N atom and CH_3 united atom were slightly changed, to allow for a simple and transferable set of partial charges. In the case of the three carboxylate ions, the carboxylate charge group was extended by one atom. Note, finally, that the 54A7 representation of the IMID ion differs slightly from that of the protonated histidine residue HISH in this force field. The reason is that HISH is alkylated while IMID presents a higher symmetry, the symmetrization requiring a slight redistribution of the atomic charges around the ring. In this symmetrized 54A7 representation, the aromatic C−H_C groups are neutral and form separate charge groups. In the 54A8 representation, however, a single charge group was retained for the entire ion, as required for a subsequent transfer to the HISH residue. More details concerning the above choices are provided in section III.1. The GROMOS 54A8 topology building blocks of the 10 ions considered are provided as a separate Supporting Information file and have been submitted to the automated topology builder and repository described in ref 94.

II.5. Ion−Solvent Radial Distribution Functions. For a given ion *I*, the ion−solvent RDF was calculated as

$$g_{IO}(r; S_I, O) = (4\pi\eta_O r^2 \Delta r)^{-1} \langle N_O(r; \Delta r) \rangle \tag{36}$$

where $\langle ... \rangle$ denotes both ensemble (trajectory) and molecule (solvent) averaging, $N_O(r;\Delta r)$ is the number of water molecules with their oxygen atom located in the distance range $r - \Delta r/2 < |\bar{\mathbf{r}}_{IO}| \leq r + \Delta r/2$ around the ion, $\bar{\mathbf{r}}_{IO}$ denoting all possible minimum-image vectors connecting the reference site S_I of the ion to the oxygen atom of any periodic copy of a water molecule, $\Delta r = 0.002$ nm is the bin width, and η_O is the water number density. The RDFs were monitored for the 10 ions considered and based on either the 54A7 or the 54A8 parameter sets. The first-peak locations can be compared to experimental estimates inferred from neutron diffraction measurements on electrolyte solutions[95−98] or, if the latter data are not available, to average ion−water hydrogen-bond lengths observed in solid crystals containing the ionic species.[99] The choice of a reference site S_I is unambiguous only for monatomic ions. For the polyatomic ions, the nitrogen atoms were chosen for H4C0, H3C1, H2C2, H1C3, H0C4, IMID, and GUAN, and the oxygen atoms were chosen for FORM, ACET, and PROP (average over all atoms of the indicated type).

II.6. Ion−Ion Potentials of Mean Force. For a given ion pair *IJ*, the ion−ion PMF is defined as

$$\zeta_{IJ}(r_{IJ}) = -N_A k_B T \ln \frac{P_{IJ}(r_{IJ})}{4\pi r_{IJ}^2} \tag{37}$$

where k_B is Boltzmann's constant and $P_{IJ}(r_{IJ})$ is the probability of occurrence of a value r_{IJ} of the interionic distance. This function was calculated by umbrella sampling[82,83] based on a series of harmonically biased simulations distributed over equidistant windows along the reaction coordinate and subsequent analysis *via* the weighted-histogram analysis method[100,101]

(WHAM). The denominator on the right-hand side of eq 37 corrects for the increase in configurational phase-space volume at increasing interionic distance r_{IJ}, i.e., corresponds to the Jacobian of the transformation from Cartesian (ion positions) to internal (interionic distance) coordinates.[102] It amounts to an additive correction $N_A k_B T[2 \ln r_{IJ} + \ln(4\pi)]$ to the "raw" PMF $\zeta_{IJ}^{raw}(r_{IJ}) = -N_A k_B T \ln P_{IJ}(r_{IJ})$. Ion−ion PMFs were calculated for the ion pairs ACET−NA, ACET−GUAN, ACET−H3C1, ACET−IMID, GUAN−CL, H3C1−CL, IMID−CL, and NA−CL, using the 54A7 and 54A8 representations of the polyatomic ions along with the sodium (NA) and chloride (CL) ion parameters of the 54A7 force field.

For each system, N_u simulations were performed with distance restraints of force constant 2500 kJ·mol^{-1}·nm^{-2} centered at interionic separations r_o ranging from $r_o(1)$ to $r_o(N_u)$ = 1.63 nm in steps of 0.07 nm. Slightly different values of $r_o(1)$ and N_u were used for the different systems, namely, 0.23 nm and 21 for the ACET−NA, H3C1−CL, and NA−CL systems; 0.30 nm and 20 for the ACET−H3C1 (54A8) and IMID−CL systems; 0.37 nm and 19 for the ACET−H3C1 (54A7), ACET−GUAN, and GUAN-CL systems; or 0.44 nm and 18 for the ACET−IMID system. To achieve sufficient overlap between successive windows, additional simulations were performed for the ACET−IMID and ACET−NA systems, with distance restraints centered at 0.545 nm (ACET−IMID) or 0.405 and 0.475 nm (ACET−NA). For the polyatomic ions, the interionic distances were measured on the basis of the carboxylate carbon atom for ACET, the carbon atom for GUAN, the nitrogen atom for H3C1, and the center of mass of the two nitrogen atoms for IMID. The PMFs were constructed over the interionic distance range from $r_o(1) - 0.15$ to 1.75 nm using the WHAM procedure with a bin width of 0.01 nm and an iteration number of 1000.

Just as was the case for single-ion hydration free energies (section II.3), the calculated ion−ion PMFs are affected by errors originating from the approximate electrostatic scheme or/and microscopic system size or/and summation scheme considered during the simulations.[87−89,103] An attempt to quantify and correct for these error sources is presented in the Supporting Information.[91,92,104] However, because the primary focus of the PMF analysis in the present context is to compare the results of the 54A7 and 54A8 force fields, for which the error is essentially identical, the curves reported in this article are not corrected for the above effects.

III. RESULTS

III.1. Reoptimization of the Nonbonded Interaction Parameters. The nonbonded interactions in the GROMOS force field are determined by an atom-type independent set of atomic partial charges q_i and an atom-type specific set of homoatomic Lennard-Jones $C_{6,ii}$ (dispersion) and $C_{12,ii}$ (repulsion) parameters. Up to three different $C_{12,ii}$ coefficients are associated with each atom type, noted $C_{12,ii}^{(1)}$, $C_{12,ii}^{(2)}$, and $C_{12,ii}^{(3)}$, and an interaction matrix M_{ij} specifying which of the three coefficients is to be used for i and for j in the (geometric-mean) combination rule defining the interaction of atom type i with atom type j. In principle, the first, second, and third coefficients correspond to nonpolar, polar-uncharged, and polar-charged interactions, respectively. Note that third-neighbor Lennard-Jones interaction parameters are defined independently, and were not altered in the present work. The changes undertaken in the charges and Lennard-Jones interaction parameters upon reoptimizing 54A7 into 54A8 are described in turn below.

Table 3. Atomic Partial Charges Used in the 54A7 and 54A8 Parameter Sets for the Ions H4C0, H3C1, H2C2, H1C3, H0C4, FORM, ACET, PROP, IMID, and GUAN[a]

atom	q_i (54A7) [e]	q_i (54A8) [e]	notes
	H4C0, H3C1, H2C2, H1C3, H0C4		
H	0.248	0.25	
C	0.127	0.20	
N	$1 - n_H(q_H - q_C) - 4q_C$		*b*
	FORM, ACET, PROP		
O	−0.635	−0.715	
C1	0.27	0.27	*c*
H	0.0	0.16	*d*
C2	0.0	0.16	*d, e*
C3	0.0	0.0	*f*
	GUAN		
C	0.34	0.01	
N	−0.26	−0.36	
H	0.24	0.345	
	IMID		
N	0.305	−0.03	*g*
H_N	0.30	0.32	*h*
C_{NN}	−0.35	0.0	*i*
H_C	0.14	0.14	*j, k*
C	−0.14	0.0	*k, l*
	HISH		
CG	−0.05	0.14	*m*
ND1	0.38	−0.03	*m*
NE2	0.31	−0.03	*m*
H_N	0.30	0.32	
CE1	−0.34	0.0	*m*
H_C	0.10	0.14	
CD2	−0.10	0.0	*m*

[a]A suggested set of partial charges for the HISH residue (protonated histidine) in the 54A8 parameter set is also provided. Unless indicated otherwise, the entire ion forms a single charge group. Note that the partial charges of IMID chosen here to investigate the properties of this ion in the 54A7 parameter set differ slightly with respect to those of the HISH residue in this force field, which is due to the requirement of symmetrizing the atomic partial charges. Abbreviations for the ion names are defined in Table 1. See also Table 2 for the corresponding Lennard-Jones interaction parameters. [b]n_H is the number of nitrogen-bound hydrogen atoms (4, 3, 2, 1, and 0 for H4C0, H3C1, H2C2, H1C3, and H0C4, respectively). [c]C1 denotes the carboxylate carbon atom. [d]This atom is a separate charge group in 54A7 but is included in the carboxylate charge group in 54A8 for FORM (H), ACET (C2), and PROP (C2). [e]C2 denotes the methyl group in the ACET ion and the methylene group in the PROP ion. [f]C3 denotes the methyl group in the PROP ion and is a separate charge group in both 54A7 and 54A8 for PROP. [g]In the HISH residue of the 54A7 force field, the two nitrogen atoms have different charges, see table entry for HISH. [h]Nitrogen-bound hydrogen atom. [i]Carbon atom between the two nitrogen atoms (in the HISH residue of the 54A7 force field, this atom has a slightly different charge, see table entry for HISH). [j]Aromatic hydrogen atom (in the HISH residue of the 54A7 force field, this atom has a slightly different charge, see table entry for HISH). [k]The aromatic C−H_C groups form separate charge groups in the 54A7 representation of IMID employed here, albeit not in the 54A8 representation and not in the HISH residue of the 54A7 force field. [l]Aromatic carbon atom (in the HISH residue of the 54A7 force field, the two aromatic carbon atoms have slightly different charges, see table entry for HISH). [m]Atom name according to the IUPAC-IUB nomenclature.[114]

The atomic partial charges of the 54A7 and 54A8 parameter sets are reported in Table 3. For the H4C0, H3C1, H2C2, H1C3, and H0C4 ions, they are similar, and the main difference

between the two sets resides in the Lennard-Jones interactions (see further below). For the FORM, ACET, and PROP ions, the positive charge on the carboxylate carbon atom C1 was retained and the negative charge on the carboxylate oxygen atoms O was enhanced from $-0.635e$ to $-0.715e$, allowing for stronger hydration of the corresponding ions (section III.2). The excess positive charge of $0.16e$ was assigned to the non-oxygen atom attached to C1 (hydrogen atom H in the case of FORM, united CH_3 or CH_2 atom in the case of ACET and PROP, respectively). This required an extension of the carboxylate charge group by one atom. Note that for the carboxylate terminus of peptides this leads to non-integer charged charge groups in GROMOS. Significant changes in the charge distribution were undertaken for the GUAN and IMID ions to allow for stronger or weaker hydration, respectively (section III.2). For GUAN, the positive charge previously residing on the carbon atom C was almost entirely removed, while the positive hydrogen H and negative nitrogen N charges were altered by $+0.105e$ and $-0.10e$, respectively, imparting a more polar character to the hydrogen-bonding NH_2 groups. For IMID, the aromatic ring, previously exhibiting a negative charge distribution, was made almost neutral. The charge of $+0.14e$ on the aromatic hydrogen atoms H_C was retained, and the charge on the nitrogen-bound hydrogen atoms H_N was slightly enhanced. The resulting ion is expected to present a reduced propensity for stacking interaction between aromatic rings. However, this deficiency is not likely to have a severe impact on (bio)molecular simulations, because (*i*) the interaction between a positively charged histidine residue and another aromatic ring generally involves a binding of the histidine protons to the π system, rather than $\pi-\pi$ stacking interactions;[105,106] (*ii*) the cation$-\pi$ interaction between a positively charged residue (e.g., a protonated lysine) and the π system of a positively charged histidine residue is hampered by the unfavorable approach of like charges; (*iii*) the mediation of stacking interactions in nonpolarizable classical atomistic force fields *via* electrostatic forces between atom-centered permanent point charges relies on a rather crude description of orbital overlap. As already pointed out in section II.4, the 54A7 parameters used here for the IMID ion are not exactly identical to those of the protonated histidine residue HISH in this force field, the most prominent difference being the use of charges $\pm 0.14e$ instead of $\pm 0.10e$ for the aromatic C$-H_C$ pairs and the assignment of these pairs to distinct charge groups. In contrast, the 54A8 IMID ion consists of one charge group, as is the case for the HISH residue in GROMOS. A suggested set of partial charges for the 54A8 HISH residue is also provided in Table 3. It is derived by transferring the charge of the replaced aromatic hydrogen atom to the carbon atom CG (C_γ).

The homoatomic Lennard-Jones interaction parameters $C_{6,ii}$ and $C_{12,ii}$ of the 54A7 and 54A8 parameter sets are reported in Table 4. Note that all atom types are identical between the two force fields, except for the methyl group in the series of methylated ammonium ions. This united atom is represented by types 16 and 54 in the 54A7 and 54A8 parameter sets, respectively. The introduction of a separate atom type for the methyl group in a positively charged entity was already a feature of the 54A7 force field in the context of phosphatidylcholine lipids.[13,24] However, this change was not applied here for the methylated ammonium ions in the 54A7 representation, which seeks analogy with the protonated lysine side chain in proteins, but it is enforced in the 54A8 representation. In addition to this change of atom type, two parameters have been altered in comparison to the 54A7 force field, both of which are solely affecting the series of ammonium ions. First, the $C_{12,ii}$ parameter of the united-atom methyl group, i.e., of atom type 54, was increased to allow for weaker hydration of the H0C4 ion (section III.2). Second, the $C_{12,ii}$ parameter of the nitrogen atom was decreased to allow for stronger hydration of the H4C0 ion (section III.2). These two changes should not affect previously parametrized molecules except phosphatidylcholine lipids. Work is in progress to test the effect of this small alteration on the properties of these lipids. The increase in the $C_{12,ii}$ parameter of atom type 54 approximately compensates for the usage, introduced in the 54A7 force field[13] on the basis of ref 24, of the $C^{(3)}_{12,ii}$ rather than the less repulsive $C^{(1)}_{12,ii}$ parameter of the phosphate oxygen atom (atom type 2) in interactions with atom type 54. Consequently, the change is reverted in the 54A8 force field, i.e. the parameter $C^{(1)}_{12,ii}$ is used again for this interaction.

III.2. Hydration Free Energies. The results of the hydration free-energy calculations for the H4C0, H3C1, H2C2, H1C3, H0C4, FORM, ACET, PROP, IMID, and GUAN ions of the 54A7 and 54A8 force fields, along with the corresponding experimental estimates (taken from Table 2), are reported in Table 5. All charging free-energy calculations were performed with both the BM and LS electrostatic schemes, the latter considering in addition two different box sizes involving 512 or 1024 water molecules. Comparison between these three estimates for each parameter set shows that methodological independence has been reached for the standard hydration free energies $\Delta G^{\ominus}_{hyd}$. For example, for the 54A8 set, the maximum differences between these estimates range from 1.1 to 2.5 kJ·mol^{-1} for the different ions. The corresponding differences in the raw charging free energies ΔG^{raw}_{chg} are significantly larger, ranging from 14.7 to 17.4 kJ·mol^{-1}.

The spreads in the three $\Delta G^{\ominus}_{hyd}$ values are essentially within the statistical error of the calculation for the cations and the FORM anion. They are still somewhat larger for the ACET and PROP ions, where the BM scheme leads to hydration free energies that are noticeably more negative compared to the LS scheme. Considering the limited differences between the two LS estimates for each ion, as well as the results of previous work on monatomic ions,[25] the LS results are probably more accurate than the BM ones. Because the effective solvent density in NPT simulations with the BM scheme is slightly higher than with the LS scheme (see $\langle L \rangle$ values in Table 5), while the solvation free energy of anions is more sensitive to this density compared to that of cations,[25] this small discrepancy is likely due to a slight oversolvation of the anions in the NPT simulations with the BM scheme.

The results of Table 5 are illustrated graphically in Figure 2. The comparison between simulated and experimental data, the latter anchored on the basis of a standard absolute intrinsic proton hydration free energy of $\Delta G^{\ominus}_{hyd}[H^+_g] = -1100$ kJ·mol^{-1}, shows that the 54A8 parameter set represents a substantial improvement over the 54A7 set in terms of the hydration free energies of the polyatomic ions. In the 54A7 force field, the H3C1 ion is correctly solvated; the H4C0, FORM, ACET, PROP, and GUAN ions are undersolvated; and the H2C2, H1C3, H0C4, and IMID ions are oversolvated. The largest error affects the ACET ion, the hydration free energy of which is off by as much as 40.0 kJ·mol^{-1}. Note that no alternative choice of $\Delta G^{\ominus}_{hyd}[H^+_g]$ could simultaneously bring the hydration free energies evaluated with the 54A7 force field to agreement with experimental conventional hydration free energies. After reparameterization of 54A7 into 54A8, the mean and maximal absolute deviations between simulated (average over the three values reported in Table 5) and experimental data over the set

Table 4. Integer Atom Codes (IAC) and Corresponding Homoatomic Lennard-Jones Dispersion and Repulsion Coefficients $C_{6,ii}$ and $C_{12,ii}$ Used in the 54A7 and 54A8 Parameter Sets for the Ions H4C0, H3C1, H2C2, H1C3, H0C4, FORM, ACET, PROP, IMID, and GUAN[a]

	54A7					54A8					
atom	IAC	$[C_{6,ii}]^{1/2}$ $[(kJ\cdot mol^{-1}\cdot nm^6)^{1/2}]$	$[C_{12,ii}^{(1)}]^{1/2}$ $[(kJ\cdot mol^{-1}\cdot nm^{12})^{1/2}]$	$[C_{12,ii}^{(2)}]^{1/2}$ $[(kJ\cdot mol^{-1}\cdot nm^{12})^{1/2}]$	$[C_{12,ii}^{(3)}]^{1/2}$ $[(kJ\cdot mol^{-1}\cdot nm^{12})^{1/2}]$	IAC	$[C_{6,ii}]^{1/2}$ $[(kJ\cdot mol^{-1}\cdot nm^6)^{1/2}]$	$[C_{12,ii}^{(1)}]^{1/2}$ $[(kJ\cdot mol^{-1}\cdot nm^{12})^{1/2}]$	$[C_{12,ii}^{(2)}]^{1/2}$ $[(kJ\cdot mol^{-1}\cdot nm^{12})^{1/2}]$	$[C_{12,ii}^{(3)}]^{1/2}$ $[(kJ\cdot mol^{-1}\cdot nm^{12})^{1/2}]$	notes
H4C0, H3C1, H2C2, H1C3, H0C4											
H	21	0	0	0	0	21	id.	id.	id.	id.	
C	16	0.09805	5.162×10^{-3}	0	0	54	id.	8.05×10^{-3}	id.	id.	*b*, *c*
	(54)	(0.09805)	(5.162×10^{-3})	(0)	(0)						*d*
N	8	0.04936	1.523×10^{-3}	3.068×10^{-3}	0	8	id.	id.	2.015×10^{-3}	id.	*e*
FORM, ACET, PROP											
O	2	0.04756	0.8611×10^{-3}	1.841×10^{-3}	3.068×10^{-3}	2	id.	id.	id.	id.	
C1	12	0.04838	2.222×10^{-3}	0	0	12	id.	id.	id.	id.	
FORM											
H	21	0	0	0	0	21	id.	id.	id.	id.	
ACET											
C2	16	0.09805	5.162×10^{-3}	0	0	16	id.	id.	id.	id.	
PROP											
C2	15	0.08642	5.828×10^{-3}	0	0	15	id.	id.	id.	id.	
C3	16	0.09805	5.162×10^{-3}	0	0	16	id.	id.	id.	id.	
GUAN											
C	12	0.04838	2.222×10^{-3}	0	0	12	id.	id.	id.	id.	
N	10	0.04936	1.523×10^{-3}	2.148×10^{-3}	0	10	id.	id.	id.	id.	
H	21	0	0	0	0	21	id.	id.	id.	id.	
IMID											
N	9	0.04936	1.523×10^{-3}	1.841×10^{-3}	0	9	id.	id.	id.	id.	
H_N	21	0	0	0	0	21	id.	id.	id.	id.	
C_{NN}	12	0.04838	2.222×10^{-3}	0	0	12	id.	id.	id.	id.	
H_C	20	0.0092	0.123×10^{-3}	0	0	20	id.	id.	id.	id.	
C	12	0.04838	2.222×10^{-3}	0	0	12	id.	id.	id.	id.	

[a] Entries "id." indicate that the corresponding interaction parameters are identical in the two parameter sets. The GROMOS force field employs up to three different $C_{12,ii}$ coefficients per atom type, noted $C_{12,ii}^{(1)}$, $C_{12,ii}^{(2)}$, and $C_{12,ii}^{(3)}$, with an associated interaction matrix M_{ij} specifying which of the three coefficients is to be used for i and j in the (geometric-mean) combination rule defining the interaction of atom type i with atom type j. In the present study, the interaction matrix of the 54A7 parameter set was used throughout, although it seems more appropriate to use the $C_{12,ii}^{(1)}$ rather than the $C_{12,ii}^{(3)}$ parameter of atom type 2 for interactions with atom type 54 in the 54A8 parameter set (section III.1). Abbreviations for the ion names are defined in Table 1. See also Table 3 for the corresponding atomic partial charges. [b] In the 54A8 parameter set, the repulsive interaction with the water oxygen atom (given by $C_{12,ii}^{(1)}$) is increased. [c] The choice of type 16 in 54A7 is motivated by analogy with the protonated lysine side chain in proteins (analogy with the phosphatidylcholine lipid headgroup would suggest type 54 instead, parameters indicated between parentheses). [d] In the 54A7 parameter set, atom types 16 and 54 differ in the repulsive interaction with atom type 2, because the latter atom type uses different $C_{12,ii}$ parameters for interaction with types 16 and 54; [e] In the 54A8 parameter set, the repulsive interaction with the water oxygen atom (given here by $C_{12,ii}^{(2)}$) is decreased.

dx.doi.org/10.1021/ct300156h | J. Chem. Theory Comput. 2012, 8, 3705−3723

Table 5. Standard Absolute Intrinsic Hydration Free Energies $\Delta G^{\ominus}_{hyd}$ of the Ions H4C0, H3C1, H2C2, H1C3, H0C4, FORM, ACET, PROP, IMID, and GUAN Calculated on the Basis of the 54A7 and 54A8 Parameter Sets (Tables 3 and 4), along with Three Different Combinations of Electrostatic Schemes (BM, LS) and System Sizes (N_w Water Molecules, Average Box-Edge Length $\langle L \rangle$)[a]

set	scheme	N_w	$\langle L \rangle$ [nm]	ΔG^{raw}_{chg} [kJ·mol^{-1}]	ΔG_{A+B+D} [kJ·mol^{-1}]	ΔG_{C_1} [kJ·mol^{-1}]	ΔG_{cav} [kJ·mol^{-1}]	$\Delta G^{\ominus}_{std}$ [kJ·mol^{-1}]	$\Delta G^{\ominus}_{hyd}$ [kJ·mol^{-1}]	exp. [kJ·mol^{-1}]
						H4C0				
54A7	BM	1024	3.16	−188.3 ± 0.5	−77.8	−75.4	15.7 ± 0.5	7.95	−317.9 ± 1.0	−344.0
54A7	LS	1024	3.17	−202.2 ± 0.6	−61.1	−76.7	15.7 ± 0.5	7.95	−316.4 ± 1.1	
54A7	LS	512	2.51	−186.2 ± 0.8	−77.2	−77.3	15.7 ± 0.5	7.95	−317.0 ± 1.4	
54A8	BM	1024	3.16	−209.5 ± 0.5	−78.1	−75.5	11.0 ± 0.5	7.95	−344.1 ± 1.0	
54A8	LS	1024	3.16	−223.6 ± 0.6	−61.7	−77.4	11.0 ± 0.5	7.95	−343.8 ± 1.1	
54A8	LS	512	2.51	−207.8 ± 0.6	−76.6	−77.3	11.0 ± 0.5	7.95	−342.8 ± 1.1	
						H3C1				
54A7	BM	1024	3.16	−173.2 ± 0.5	−77.7	−75.4	11.2 ± 0.7	7.95	−307.1 ± 1.2	−307.1
54A7	LS	1024	3.17	−186.8 ± 0.6	−61.3	−76.7	11.2 ± 0.7	7.95	−305.6 ± 1.3	
54A7	LS	512	2.51	−171.6 ± 0.8	−76.7	−77.3	11.2 ± 0.7	7.95	−306.4 ± 1.5	
54A8	BM	1024	3.16	−177.4 ± 0.6	−77.8	−75.4	13.7 ± 0.8	7.95	−308.9 ± 1.3	
54A8	LS	1024	3.17	−191.4 ± 0.6	−61.2	−76.7	13.7 ± 0.8	7.95	−307.6 ± 1.3	
54A8	LS	512	2.51	−176.2 ± 0.6	−76.5	−77.3	13.7 ± 0.8	7.95	−308.3 ± 1.3	
						H2C2				
54A7	BM	1024	3.16	−152.9 ± 0.4	−77.6	−75.3	9.6 ± 1.0	7.95	−288.1 ± 1.4	−274.5
54A7	LS	1024	3.17	−166.7 ± 0.6	−61.3	−76.7	9.6 ± 1.0	7.95	−287.1 ± 1.5	
54A7	LS	512	2.52	−151.4 ± 0.7	−76.2	−76.3	9.6 ± 1.0	7.95	−286.3 ± 1.7	
54A8	BM	1024	3.16	−145.4 ± 0.4	−77.5	−75.2	18.6 ± 1.0	7.95	−271.4 ± 1.5	
54A8	LS	1024	3.17	−159.9 ± 0.5	−61.1	−76.7	18.6 ± 1.0	7.95	−271.1 ± 1.6	
54A8	LS	512	2.52	−144.5 ± 0.5	−76.0	−76.3	18.6 ± 1.0	7.95	−270.3 ± 1.5	
						H1C3				
54A7	BM	1024	3.16	−128.8 ± 0.4	−77.4	−75.2	4.5 ± 1.0	7.95	−268.9 ± 1.4	−243.1
54A7	LS	1024	3.17	−142.8 ± 0.5	−61.1	−76.7	4.5 ± 1.0	7.95	−268.1 ± 1.5	
54A7	LS	512	2.52	−127.6 ± 0.6	−75.9	−76.3	4.5 ± 1.0	7.95	−267.4 ± 1.6	
54A8	BM	1024	3.16	−115.9 ± 0.4	−77.1	−75.0	17.3 ± 1.0	7.95	−242.7 ± 1.4	
54A8	LS	1024	3.17	−129.6 ± 0.5	−60.5	−76.7	17.3 ± 1.0	7.95	−241.6 ± 1.5	
54A8	LS	512	2.52	−114.6 ± 0.5	−75.6	−76.3	17.3 ± 1.0	7.95	−241.3 ± 1.5	
						H0C4				
54A7	BM	1024	3.16	−100.6 ± 0.3	−77.2	−75.1	3.1 ± 1.0	7.95	−241.9 ± 1.4	−211.1
54A7	LS	1024	3.17	−114.3 ± 0.5	−60.8	−76.7	3.1 ± 1.0	7.95	−240.8 ± 1.5	
54A7	LS	512	2.52	−99.6 ± 0.5	−75.7	−76.3	3.1 ± 1.0	7.95	−240.5 ± 1.5	
54A8	BM	1024	3.16	−88.1 ± 0.4	−76.7	−74.9	18.6 ± 1.3	7.95	−213.2 ± 1.6	
54A8	LS	1024	3.17	−101.7 ± 0.4	−60.7	−76.7	18.6 ± 1.3	7.95	−212.5 ± 1.6	
54A8	LS	512	2.52	−87.0 ± 0.4	−75.2	−76.3	18.6 ± 1.3	7.95	−211.9 ± 1.7	
						FORM				
54A7	BM	1024	3.16	−299.1 ± 0.6	−77.6	75.4	10.9 ± 0.8	7.95	−282.4 ± 1.4	−315.4
54A7	LS	1024	3.16	−316.9 ± 0.7	−61.4	77.4	10.9 ± 0.8	7.95	−282.0 ± 1.5	
54A7	LS	512	2.51	−300.9 ± 1.0	−76.2	77.3	10.9 ± 0.8	7.95	−281.0 ± 1.8	
54A8	BM	1024	3.16	−331.6 ± 0.7	−77.8	75.4	10.9 ± 0.8	7.95	−315.1 ± 1.4	
54A8	LS	1024	3.16	−349.0 ± 0.7	−61.4	77.4	10.9 ± 0.8	7.95	−314.1 ± 1.5	
54A8	LS	512	2.51	−333.4 ± 0.7	−76.3	77.3	10.9 ± 0.8	7.95	−313.6 ± 1.4	
						ACET				
54A7	BM	1024	3.16	−298.3 ± 0.6	−77.6	75.2	10.2 ± 0.9	7.95	−282.6 ± 1.5	−321.2
54A7	LS	1024	3.16	−315.1 ± 0.7	−61.3	77.4	10.2 ± 0.9	7.95	−280.9 ± 1.6	
54A7	LS	512	2.51	−299.2 ± 0.9	−76.4	77.3	10.2 ± 0.9	7.95	−280.2 ± 1.8	
54A8	BM	1024	3.16	−340.0 ± 0.6	−77.9	75.2	10.2 ± 0.9	7.95	−324.5 ± 1.5	
54A8	LS	1024	3.16	−356.7 ± 0.8	−61.5	77.4	10.2 ± 0.9	7.95	−322.6 ± 1.7	
54A8	LS	512	2.51	−340.8 ± 0.7	−76.6	77.3	10.2 ± 0.9	7.95	−322.0 ± 1.6	
						PROP				
54A7	BM	1024	3.16	−296.9 ± 0.6	−77.6	75.2	10.8 ± 0.8	7.95	−280.5 ± 1.4	−315.4
54A7	LS	1024	3.17	−314.0 ± 0.8	−61.1	76.7	10.8 ± 0.8	7.95	−279.6 ± 1.6	
54A7	LS	512	2.51	−299.3 ± 0.9	−76.6	77.3	10.8 ± 0.8	7.95	−279.9 ± 1.7	
54A8	BM	1024	3.16	−339.1 ± 0.6	−77.8	75.2	10.8 ± 0.8	7.95	−323.0 ± 1.4	
54A8	LS	1024	3.17	−355.5 ± 0.7	−61.2	76.7	10.8 ± 0.8	7.95	−321.3 ± 1.6	
54A8	LS	512	2.51	−340.1 ± 0.7	−76.9	77.3	10.8 ± 0.8	7.95	−320.9 ± 1.6	

Table 5. continued

set	scheme	N_w	$\langle L \rangle$ [nm]	ΔG^{raw}_{chg} [kJ·mol^{-1}]	ΔG_{A+B+D} [kJ·mol^{-1}]	ΔG_{C_1} [kJ·mol^{-1}]	ΔG_{cav} [kJ·mol^{-1}]	$\Delta G^{\ominus}_{std}$ [kJ·mol^{-1}]	$\Delta G^{\ominus}_{hyd}$ [kJ·mol^{-1}]	exp. [kJ·mol^{-1}]
						IMID				
54A7	BM	1024	3.16	−138.1 ± 0.5	−76.9	−75.2	5.7 ± 0.9	7.95	−276.6 ± 1.4	−263.9
54A7	LS	1024	3.17	−152.0 ± 0.7	−61.0	−76.7	5.7 ± 0.9	7.95	−276.1 ± 1.6	
54A7	LS	512	2.52	−136.9 ± 0.7	−75.8	−76.3	5.7 ± 0.9	7.95	−275.4 ± 1.6	
54A8	BM	1024	3.16	−125.3 ± 0.4	−76.9	−75.2	5.7 ± 0.9	7.95	−263.8 ± 1.3	
54A8	LS	1024	3.17	−139.7 ± 0.6	−60.9	−76.7	5.7 ± 0.9	7.95	−263.7 ± 1.5	
54A8	LS	512	2.52	−124.2 ± 0.8	−75.8	−76.3	5.7 ± 0.9	7.95	−262.7 ± 1.7	
						GUAN				
54A7	BM	1024	3.16	−125.8 ± 0.4	−77.0	−75.2	15.6 ± 0.9	7.95	−254.3 ± 1.3	−269.0
54A7	LS	1024	3.17	−140.1 ± 0.7	−61.1	−76.7	15.6 ± 0.9	7.95	−254.3 ± 1.6	
54A7	LS	512	2.52	−124.8 ± 0.6	−75.9	−76.3	15.6 ± 0.9	7.95	−253.4 ± 1.5	
54A8	BM	1024	3.16	−140.6 ± 0.5	−76.7	−75.2	15.6 ± 0.9	7.95	−268.9 ± 1.4	
54A8	LS	1024	3.17	−155.2 ± 0.8	−61.2	−76.7	15.6 ± 0.9	7.95	−269.5 ± 1.7	
54A8	LS	512	2.52	−139.6 ± 0.8	−75.8	−76.3	15.6 ± 0.9	7.95	−268.2 ± 1.7	

[a]The standard hydration free energy $\Delta G^{\ominus}_{hyd}$ (eq 35) is calculated as a sum of the raw charging free energy ΔG^{raw}_{chg} (section II.3.2), the correction terms ΔG_{A+B+D} and ΔG_{C_1} (eqs 25, 26, 31, and 32), the cavitation free energy ΔG_{cav} (section II.3.2), and the standard-state conversion term $\Delta G^{\ominus}_{std}$ (eq 4). The experimental values ("exp.") are reported from Table 2. Abbreviations for the ion names are defined in Table 1.

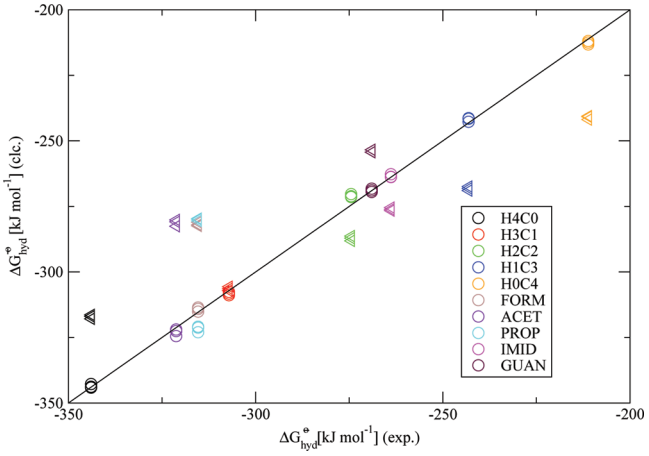

Figure 2. Standard absolute intrinsic hydration free energies $\Delta G^{\ominus}_{hyd}$ of the ions H4C0, H3C1, H2C2, H1C3, H0C4, FORM, ACET, PROP, IMID, and GUAN calculated ("clc."; Table 5) based on the 54A7 (triangles; multiple instances corresponding to the different electrostatic schemes and numbers of water molecules as reported in Table 5) and 54A8 (circles; multiple instances corresponding to the different electrostatic schemes and numbers of water molecules as reported in Table 5) parameter sets (Tables 3 and 4), along with corresponding experimental estimates ("exp."; Table 2 or 5). The line represents the ideal situation $\Delta G^{\ominus}_{hyd}$(clc.) = $\Delta G^{\ominus}_{hyd}$(exp.). Abbreviations for the ion names are defined in Table 1.

of 10 ions are reduced from 23.1 and 40.0 kJ·mol^{-1}, respectively, to 1.8 and 6.3 kJ·mol^{-1}, respectively.

III.3. Ion−Solvent Radial Distribution Functions. The 54A7 and 54A8 parameter sets were further compared in terms of structural ion−water binding properties. Table 6 lists the locations R_{rdf} of the first peaks in the ion−water RDFs (eq 36) along with corresponding experimental estimates. Note that the experimental data for the H3C1 and IMID ions are an estimate for the average hydrogen-bond length with water[99] (distance between donor and acceptor atoms) rather than for the location of the first peak in the ion−water RDF. Overall, the results of the 54A7 and 54A8 force fields are both in good agreement with experimental results and quite similar to each other, except for the H4C0, H3C1, H2C2, H1C3, H0C4, and GUAN ions, where noticeable differences are observed between the two force fields. For the ammonium ion series, the 54A8 force field reproduces the experimental data better. While the 54A7 parameter set overestimates the size of the first four ions in this series, it underestimates the size of the tetramethylated species. This trend is also reflected in the corresponding hydration free energies (Table 5). Note that for the H3C1 ion, the hydration free energy based on the 54A7 force field is in agreement with experimental data, but R_{rdf} is still overestimated by 0.009 nm. Due to the decreased repulsion between the nitrogen atom and the water oxygen atom in the 54A8 force field, R_{rdf} of H3C1 is now slightly underestimated by 0.003 nm. The experimental value of R_{rdf} for the GUAN ion is a relatively crude estimate, being based on an assumed N−H−O angle of 180°.[98] The 54A7 parameter set overestimates this value by 0.013 nm, while the 54A8 parameter set underestimates it by 0.014 nm.

III.4. Ion−Ion Potentials of Mean Force. In view of the importance of ionic hydration free energies in the context of ion pairing (law of "matching water affinities"[42,45,46,107,108]), failure to account for relative ionic hydration free energies in the 54A7 force field (section III.2) might impair the description of ion−ion association properties. In turn, incorrect ion−ion association properties may affect the description of salt-bridge formation and ionic cosolute-binding in the context of biomolecules. Therefore, the 54A7 and 54A8 parameter sets were further compared in terms of ion−ion binding properties. Figure 3 shows the PMFs for a selected set of oppositely charged ion pairs, according to the 54A7 and 54A8 representations. The considered ion pairs also involve the NA and CL ions, which are widely used counterions in (bio)molecular simulations. Although the PMF curves calculated here, due to the consideration of a single ion pair at infinite dilution in a solvent of high relative dielectric permittivity (water), are not appropriate for drawing conclusions concerning ionic binding properties inside or at the surface of a biomolecule (the corresponding environment being characterized by a lower effective dielectric permittivity[109−111]), they serve to establish a comparison between the two force fields and to assess possible differences in ion−ion binding strengths.

Table 6. Experimental Estimates and Simulated Results for the Position R_{rdf} of the First Peak in the Ion−Water (Oxygen) Radial Distribution Function (RDF)[a]

ion	reference atom	R_{rdf} (54A7) [nm]	R_{rdf} (54A8) [nm]	R_{rdf} (exp.) [nm]	ref.	notes
H4C0	N	0.295	0.281	0.285	95	
H3C1	N	0.293	0.281	[0.284]	99	*b*
H2C2	N	0.293	0.281			
H1C3	N	0.291	0.283			
H0C4	N	0.456	0.477	0.47	96	
FORM	O	0.283	0.280			
ACET	O	0.283	0.280	0.282−0.288	97	
PROP	O	0.283	0.280			
IMID	N	0.273	0.277	[0.273]	99	*b*
GUAN	N	0.313	0.286	∼0.3	98	*c*

[a]Radial distribution functions $g_{IO}(r)$ were calculated according to eq 36 using the 54A7 and 54A8 parameter sets (Tables 3 and 4), based on simulations employing the BM scheme (section II.2). The experimental data were taken from the indicated sources. Values in square brackets correspond to average ion−water hydrogen-bond lengths (distance between donor and acceptor atoms) observed in solid crystals containing the ionic species. Abbreviations for the ion names are defined in Table 1. [b]The experimental values ("exp.") are an average hydrogen-bond length with water (distance between donor and acceptor atoms), as observed in a solid crystal containing the indicated ionic species. [c]Approximate estimate.

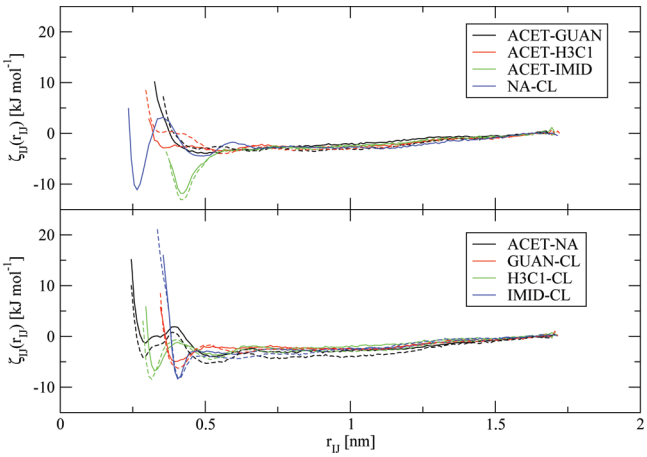

Figure 3. Potentials of mean force $\zeta_{IJ}(r_{IJ})$ for ion−ion association in water, monitored along the interionic distance r_{IJ} for selected oppositely charged ion pairs considered in this study. Solid and dashed lines correspond to results using the 54A7 and 54A8 parameter sets, respectively (Tables 3 and 4), based on simulations employing the BM scheme (section II.2). The models for NA and CL are the same in both parameter sets. The PMF curves were calculated according to eq 37, and were anchored to zero at r_{IJ} = 1.635 nm. Abbreviations for the ion names are defined in Table 1.

On the basis of the PMF, the free energy necessary to separate a contact ion pair can be estimated by the free energy of the water-bridged (second minimum) relative to the contact (first minimum) ion pair. In terms of this property, the only significant difference between the two force-field representations is found for the ACET-H3C1 ion pair, where the 54A8 force field destabilizes the contact ion pair compared to the 54A7 force field. In both force fields, the region separating the two configurations does not exhibit a clear-cut maximum so that it is difficult to discern the exact location of the first minimum. Choosing interionic separations of 0.361 and 0.348 nm as the locations of the contact minimum in the 54A7 and 54A8 force fields, respectively, along with distances of 0.581 and 0.562 nm, respectively, for the water-bridged one, free energy differences between the two configurations amount to 0.5 and 4.2 kJ·mol^{-1}, respectively. This difference is likely due to the increased hydrophilicity of the ACET ion in the 54A8 force field, implying a larger desolvation penalty, and the increased repulsion between the methyl group of the H3C1 ion and the oxygen atoms of the ACET ion.

Comparing the PMFs among each other, the ACET−IMID ion pair appears to be exceptionally stable in comparison to the other molecular-ion pairs. The free energy differences between interionic separations of 0.42 nm (contact ion pair) and 0.90 nm (separated ion pair; a second minimum indicating a water-bridged ion pair is not clearly discernible here) are about −9.1 and −10.2 kJ·mol^{-1} in the 54A7 and 54A8 force fields, respectively.

IV. CONCLUSION

The aim of the present work was threefold (points 1−3 in section I), and the conclusions reached in this study can be summarized accordingly as follows:

1. Assuming a value $\Delta G^{\ominus}_{hyd}[H^+_g]$ = −1100 kJ·mol^{-1} for the absolute intrinsic hydration free energy of the proton, the 54A7 parameter set only appropriately reproduces experimental data in the case of the H3C1 ion, which represents the tailing functional group of the charged lysine side chain. For the other ions, the calculated hydration free energy is either underestimated (H4C0, FORM, ACET, PROP, GUAN) or overestimated (H2C2, H1C3, H0C4, IMID) in magnitude, the largest deviation affecting the ACET ion (40.0 kJ·mol^{-1}), which represents the tailing functional group of the charged aspartate and glutamate side chains. No alternative choice of $\Delta G^{\ominus}_{hyd}[H^+_g]$ can bring the hydration free energies evaluated with the 54A7 force field to simultaneously agree with experimental conventional hydration free energies.
2. The nonbonded interaction parameters of the charged amino acid side chain analogs were reoptimized against experimental absolute intrinsic hydration free energies to yield a new parameter set 54A8. The required experimental estimates for the conventional hydration free energies of the H4C0, H3C1, H2C2, H1C3, H0C4, FORM, ACET, PROP, IMID, and GUAN ions were derived on the basis of raw data from refs 32, 53, 54, 57, 58, and 61 and combined with $\Delta G^{\ominus}_{hyd}[H^+_g]$ = −1100 kJ·mol^{-1}, to yield absolute intrinsic hydration free energies which served as experimental reference data. The raw computed hydration free energies are affected by approximate electrostatic, finite-size, and potential-summation artifacts but were corrected for methodological dependence along the line of previous studies performed in the context of monatomic ions.[25,26] After reparameterization of 54A7 into 54A8, the mean and maximal absolute deviations between simulated and experimental data over the set of 10 ions are reduced from 23.1 and 40.0 kJ·mol^{-1}, respectively, to 1.8 and 6.3 kJ·mol^{-1}, respectively.
3. An initial validation of the 54A8 parameter set against properties other than single-ion hydration free energies, namely, ion−water RDFs and ion−ion PMFs, was also

undertaken. Structural properties of water around ions, as represented by experimentally inferred first peak positions in the ion−water RDFs (or average ion−water hydrogen-bond lengths in case the former data were not available), are found to be well reproduced in the two force-field representations, 54A8 performing slightly better in the case of the methylated ammonium ions. For the ion−ion PMFs, very similar results are also obtained for the two parameter sets. The only notable difference is found for the ACET-H3C1 pair, where the 54A8 parameter set leads to a destabilization of the contact ion pair by about 3.7 kJ·mol^{-1} compared to the 54A7 force field.

A number of points should be kept in mind concerning the applicability of the 54A8 force-field version developed in this article, which will have to be addressed in future work, namely:

A. The charged amino acid side chain analogs of the 54A8 parameter set might not be compatible with other charged groups of the 54A7 force field, which have not yet been parametrized against methodology-independent hydration free energies. For example, it will be necessary to also reparameterize other important monatomic (e.g., Ca^{2+}, Mg^{2+}) and polyatomic (e.g., PO_4^{3-}, CO_3^{2-}, SO_4^{2-}) ions in a similar fashion. In addition, the performance of the new description of charged functional groups will have to be tested in biomolecular simulations involving proteins, nucleic acids, carbohydrates, and lipids, so as to verify whether the new force field still achieves a realistic representation of biomolecular structure and dynamics (e.g., salt-bridge formation, pH sensitivity) and Hofmeister effects (e.g., denaturating effect of guanidinium chloride). Work is in progress along these lines.

B. The current parametrization was targeted at properties of ions in the infinitely dilute regime. Since the GROMOS force field uses a simple geometric-mean combination rule to translate Lennard-Jones interaction parameters valid in a system governed by few heteroatomic interactions (e.g., ion−water) to complex entities involving numerous types of heteroatomic interactions (e.g., ion−ion, ion-protein), it is not *a priori* clear whether the parameters of the polyatomic ions in the 54A8 force field can be successfully transferred to an environment characterized by multiple interactions with species and functional groups other than water. In particular, the accurate description of both infinite-dilution and finite-concentration properties is highly desirable in terms of force-field performance.

C. The use of charged functional groups parametrized against methodology-independent hydration free energies, i.e., calibrated for the ideal situation of Coulombic electrostatic interactions in a macroscopic nonperiodic system, in simulations where these groups are actually propagated with approximate electrostatic interactions within systems of finite sizes, might strongly affect the configurational sampling. Owing to the predominantly negative correction terms, the ions may in practice be underhydrated in real simulations, the effect being more severe for cations (negative type-C_1 correction) than for anions (positive type-C_1 correction), and presumably also more severe for monatomic ions (concentrated charge density) compared to polyatomic ones (more diffuse charge density). The decreased effective hydrophilicity of the charged functional groups might cause an overestimation of ion−ion binding in solution, or an underestimation of the interaction of protein side chains with the solvent. It would therefore be desirable to design new effective electrostatic interaction schemes which correct the approximate electrostatics and finite-size effects at the level of the forces, so as to achieve a solvent polarization around ionic groups that is exempt of artifacts.

Clearly, the calibration of charged species and functional groups in the context of (bio)molecular force fields is a very intricate problem, and the 54A8 force field remains to be more extensively validated against other sources of experimental data, as well as extended to other types of ions and charged functional groups. However, the authors believe that the present work represents an important step in providing the foundation for thermodynamics-based approaches to the problem, far superior to previous approaches relying mainly on chemical intuition and common sense.

■ ASSOCIATED CONTENT

Supporting Information

Building blocks for all polyatomic ions, as well as additional details concerning the choice of effective ionic volume, the correction for the solute self-exclusion potential, and corrections to the ion−ion PMF are provided. This material is available free of charge via the Internet at http://pubs.acs.org.

■ AUTHOR INFORMATION

Corresponding Author

*Phone: +43 1 476548302. Fax: +43 1 476548309. E-mail: chris.oostenbrink@boku.ac.at.

Notes

The authors declare no competing financial interest.

■ ACKNOWLEDGMENTS

Financial support from Project No. M1281-N17 of the Austrian Science Fund (FWF), Grant No. LS08-QM3 of the Vienna Science and Technology Fund (WWTF), Grant No. 260408 of the European Research Council (ERC), and Grant No. 20021−138020 of the Swiss National Science Foundation (SNF) are gratefully acknowledged.

■ DEDICATION

The authors would like to dedicate this article to Wilfred van Gunsteren in the honor of his 65th birthday, and express him their gratitude for long-standing supervision, support, and friendship. We are very happy to add to his continuous work on the GROMOS force field with the present parameter set.

■ REFERENCES

(1) Allen, M. P.; Tildesley, D. J. *Computer Simulation of Liquids*; Oxford University Press: New York, 1987.

(2) van Gunsteren, W. F.; Berendsen, H. J. C. *Angew. Chem., Int. Ed.* **1990**, *29*, 992−1023.

(3) Berendsen, H. J. C. *Simulating the Physical World*; Cambridge University Press: Cambridge, U.K., 2007.

(4) Hünenberger, P. H.; Reif, M. M. *Single-Ion Solvation: Experimental and Theoretical Approaches to Elusive Thermodynamic Quantities*; Royal Society of Chemistry: London, U.K., 2011; Theoretical and Computational Chemistry Series.

(5) Hermans, J.; Berendsen, H. J. C.; van Gunsteren, W. F.; Postma, J. P. M. *Biopolymers* **1984**, *23*, 1513−1518.

(6) van Gunsteren, W. F.; Billeter, S. R.; Eising, A. A.; Hünenberger, P. H.; Krüger, P.; Mark, A. E.; Scott, W. R. P.; Tironi, I. G. *Biomolecular simulation: The GROMOS96 manual and user guide*; Verlag der Fachvereine: Zürich, Switzerland, 1996.
(7) Schuler, L. D.; van Gunsteren, W. F. *Mol. Simul.* **2000**, *25*, 301−319.
(8) Schuler, L. D.; Daura, X.; van Gunsteren, W. F. *J. Comput. Chem.* **2001**, *22*, 1205−1218.
(9) Lins, R. D.; Hünenberger, P. H. *J. Comput. Chem.* **2005**, *26*, 1400−1412.
(10) Oostenbrink, C.; Villa, A.; Mark, A. E.; van Gunsteren, W. F. *J. Comput. Chem.* **2004**, *25*, 1656−1676.
(11) Hansen, H. S.; Hünenberger, P. H. *J. Comput. Chem.* **2011**, *32*, 998−1032.
(12) Horta, B. A. C.; Fuchs, P. F. J.; van Gunsteren, W. F.; Hünenberger, P. H. *J. Chem. Theory Comput.* **2011**, *7*, 1016−1031.
(13) Schmid, N.; Eichenberger, A. P.; Choutko, A.; Riniker, S.; Winger, M.; Mark, A. E.; van Gunsteren, W. F. *Eur. Biophys. J.* **2011**, *40*, 843−856.
(14) Mie, G. *Ann. Phys.* **1903**, *316*, 657−697.
(15) Jones, J. E. *Proc. R. Soc. London, Ser. A* **1924**, *106*, 441−462.
(16) Jones, J. E. *Proc. R. Soc. London, Ser. A* **1924**, *106*, 463−477.
(17) Berendsen, H. J. C.; Postma, J. P. M.; van Gunsteren, W. F.; Hermans, J. Interaction models for water in relation to protein hydration. In *Intermolecular Forces*; Pullman, B., Ed.; Reidel: Dordrecht, The Netherlands, 1981; pp 331−342.
(18) Barker, J. A.; Watts, R. O. *Mol. Phys.* **1973**, *26*, 789−792.
(19) van Gunsteren, W. F.; Karplus, M. *Macromolecules* **1982**, *15*, 1528−1544.
(20) Daura, X.; Mark, A. E.; van Gunsteren, W. F. *J. Comput. Chem.* **1998**, *19*, 535−547.
(21) Chandrasekhar, I.; Kastenholz, M. A.; Lins, R. D.; Oostenbrink, C.; Schuler, L. D.; Tieleman, D. P.; van Gunsteren, W. F. *Eur. Biophys. J.* **2003**, *32*, 67−77.
(22) Soares, T. A.; Hünenberger, P. H.; Kastenholz, M. A.; Kräutler, V.; Lenz, T.; Lins, R. D.; Oostenbrink, C.; van Gunsteren, W. F. *J. Comput. Chem.* **2005**, *26*, 725−737.
(23) Horta, B. A. C.; Lin, Z.; Huang, W.; Riniker, S.; van Gunsteren, W. F.; Hünenberger, P. H. *J. Comput. Chem.*, in press.
(24) Poger, D.; van Gunsteren, W. F.; Mark, A. E. *J. Comput. Chem.* **2009**, *31*, 1117−1125.
(25) Reif, M. M.; Hünenberger, P. H. *J. Chem. Phys.* **2011**, *134*, 144104/1−144104/25.
(26) Kastenholz, M. A.; Hünenberger, P. H. *J. Chem. Phys.* **2006**, *124*, 224501/1−224501/20.
(27) Tawa, G. J.; Topol, I. A.; Burt, S. K.; Caldwell, R. A.; Rashin, A. A. *J. Chem. Phys.* **1998**, *109*, 4852−4863.
(28) Pliego, J. R.; Riveros, J. M. *Chem. Phys. Lett.* **2000**, *332*, 597−602.
(29) Pliego, J. R.; Riveros, J. M. *J. Phys. Chem. B* **2000**, *104*, 5155−5160.
(30) Pliego, J. R.; Riveros, J. M. *J. Chem. Phys.* **2000**, *112*, 4045−4052.
(31) Camaioni, D. M.; Schwerdtfeger, C. A. *J. Phys. Chem. A* **2005**, *109*, 10795−10797.
(32) Kelly, C. P.; Cramer, C. J.; Truhlar, D. G. *J. Phys. Chem. B* **2006**, *110*, 16066−16081.
(33) Tissandier, M. D.; Cowen, K. A.; Feng, W. Y.; Gundlach, E.; Cohen, M. H.; Earhart, A. D.; Coe, J. V.; Tuttle, T. R., Jr. *J. Phys. Chem. A* **1998**, *102*, 7787−7794.
(34) Tissandier, M. D.; Cowen, K. A.; Feng, W. Y.; Gundlach, E.; Cohen, M. H.; Earhart, A. D.; Coe, J. V.; Tuttle, T. R., Jr. *J. Phys. Chem. A* **1998**, *102*, 9308−9308.
(35) Isse, A. A.; Gennaro, A. *J. Phys. Chem. B* **2010**, *114*, 7894−7899.
(36) Bartmess, J. E. *J. Phys. Chem.* **1994**, *98*, 6420−6424.
(37) Kastenholz, M. A.; Hünenberger, P. H. *J. Chem. Phys.* **2006**, *124*, 124106/1−124106/27.
(38) Reif, M. M.; Hünenberger, P. H. *J. Chem. Phys.* **2011**, *134*, 144103/1−144103/30.
(39) Slater, J. C.; Kirkwood, J. G. *Phys. Rev.* **1931**, *37*, 682−697.
(40) Cacace, M. G.; Landau, E. M.; Ramsden, J. J. *Q. Rev. Biophys.* **1997**, *30*, 241−277.
(41) Kunz, W.; Lo Nostro, P.; Ninham, B. W. *Curr. Opin. Colloid Interface Sci.* **2004**, *9*, 1−18.
(42) Collins, K. D. *Biophys. Chem.* **2006**, *119*, 271−281.
(43) Jungwirth, P.; Tobias, D. J. *Chem. Rev.* **2006**, *106*, 1259−1281.
(44) Zhang, Y.; Cremer, P. S. *Curr. Opin. Chem. Biol.* **2006**, *10*, 658−663.
(45) Collins, K. D.; Neilson, G. W.; Enderby, J. E. *Biophys. Chem.* **2007**, *128*, 95−104.
(46) Vlachy, N.; Jagoda-Cwiklik, B.; Vácha, R.; Touraud, D.; Jungwirth, P.; Kunz, W. *Adv. Colloid Interface Sci.* **2008**, *146*, 42−47.
(47) Kirkwood, J. G.; Buff, F. P. *J. Chem. Phys.* **1951**, *19*, 774−777.
(48) Ben-Naim, A. *Molecular Theory of Solutions*; Oxford University Press: Oxford, U.K., 2006.
(49) Weerasinghe, S.; Smith, P. E. *J. Chem. Phys.* **2003**, *119*, 11342−11349.
(50) Klasczyk, B.; Knecht, V. *J. Chem. Phys.* **2010**, *132*, 024109/1−024109/12.
(51) Lide, D. R. *CRC Handbook of Chemistry and Physics*, ed. 83; CRC Press: Boca Raton, FL, 2002.
(52) Tuttle, T. R., Jr.; Malaxos, S.; Coe, J. V. *J. Phys. Chem. A* **2002**, *106*, 925−932.
(53) Nagano, Y.; Sakiyama, M.; Fujiwara, T.; Kondo, Y. *J. Phys. Chem.* **1988**, *92*, 5823−5827.
(54) Marcus, Y. *Ion Properties*; Marcel Dekker, Inc.: New York, 1997.
(55) Loewenschuss, A.; Marcus, Y. *J. Phys. Chem. Ref. Data* **1987**, *16*, 61−89.
(56) Hunter, E. P. L.; Lias, S. G. *J. Phys. Chem. Ref. Data* **1998**, *27*, 413−656.
(57) Linstrom, P. J.; Mallard, W. G. *NIST Chemistry WebBook, NIST standard reference database number 69*; National Institute of Standards and Technology: Gaithersburg, MD, 2009. Available at http://webbook.nist.gov (accessed Apr. 2012).
(58) Klicić, J. J.; Friesner, R. A.; Liu, S.-Y.; Guida, W. C. *J. Phys. Chem. A* **2002**, *106*, 1327−1335.
(59) Pearson, R. G. *J. Am. Chem. Soc.* **1986**, *108*, 6109−6114.
(60) Wolfenden, R.; Andersson, L.; Cullis, P. M.; Southgate, C. C. B. *Biochemistry* **1981**, *20*, 849−855.
(61) Marenich, A. V.; Kelly, C. P.; Thompson, J. D.; Hawkins, G. D.; Chambers, C. C.; Giesen, D. J.; Winget, P.; Cramer, C. J.; Truhlar, D. G. *Minnesota Solvation Database*, version 2009; University of Minnesota: Minneapolis, MN, 2009. Available at http://comp.chem.umn.edu/mnsol (accessed Apr. 2012).
(62) Perrin, D. D. *Dissociation constants of organic bases in aqueous solution (Supplement 1972)*; Butterworths: London, U.K., 1965.
(63) Scott, W. R. P.; Hünenberger, P. H.; Tironi, I. G.; Mark, A. E.; Billeter, S. R.; Fennen, J.; Torda, A. E.; Huber, T.; Krüger, P.; van Gunsteren, W. F. *J. Phys. Chem. A* **1999**, *103*, 3596−3607.
(64) Schmid, N.; Christ, C. D.; Christen, M.; Eichenberger, A. P.; van Gunsteren, W. F. *Comput. Phys. Commun.* **2012**, *183*, 890−903.
(65) Hockney, R. W.; Eastwood, J. W. *Computer Simulation Using Particles*; McGraw-Hill: New York, 1981.
(66) Hünenberger, P. H. Lattice-sum methods for computing electrostatic interactions in molecular simulations. In *Simulation and Theory of Electrostatic Interactions in Solution: Computational Chemistry, Biophysics, and Aqueous Solution*; Hummer, G., Pratt, L. R., Eds.; American Institute of Physics: New York, 1999; pp 17−83.
(67) Hockney, R. W. *Methods Comput. Phys.* **1970**, *9*, 136−211.
(68) Ryckaert, J.-P.; Ciccotti, G.; Berendsen, H. J. C. *J. Comput. Phys.* **1977**, *23*, 327−341.
(69) Berendsen, H. J. C.; Postma, J. P. M.; van Gunsteren, W. F.; di Nola, A.; Haak, J. R. *J. Chem. Phys.* **1984**, *81*, 3684−3690.
(70) Kell, G. S. *J. Chem. Eng. Data* **1967**, *12*, 66−69.
(71) Glättli, A.; Daura, X.; van Gunsteren, W. F. *J. Chem. Phys.* **2002**, *116*, 9811−9828.
(72) Christen, M.; Hünenberger, P. H.; Bakowies, D.; Baron, R.; Bürgi, R.; Geerke, D. P.; Heinz, T. N.; Kastenholz, M. A.; Kräutler, V.;

Oostenbrink, C.; Peter, C.; Trzesniak, D.; van Gunsteren, W. F. *J. Comput. Chem.* **2005**, *26*, 1719−1751.
(73) Heinz, T. N.; Hünenberger, P. H. *J. Chem. Phys.* **2005**, *123*, 034107/1−034107/19.
(74) Hünenberger, P. H. *J. Chem. Phys.* **2000**, *113*, 10464−10476.
(75) Deserno, M.; Holm, C. *J. Chem. Phys.* **1998**, *109*, 7678−7693.
(76) Deserno, M.; Holm, C. *J. Chem. Phys.* **1998**, *109*, 7694−7701.
(77) Redlack, A.; Grindlay, J. *Can. J. Phys.* **1972**, *50*, 2815−2825.
(78) Nijboer, B. R. A.; Ruijgrok, T. W. *J. Stat. Phys.* **1988**, *53*, 361−382.
(79) Hummer, G.; Pratt, L. R.; Garcia, A. E. *J. Phys. Chem.* **1996**, *100*, 1206−1215.
(80) Bogusz, S.; Cheatham, T. E.; Brooks, B. R. *J. Chem. Phys.* **1998**, *108*, 7070−7084.
(81) Kirkwood, J. G. *J. Chem. Phys.* **1935**, *3*, 300−313.
(82) Torrie, G. M.; Valleau, J. P. *J. Comput. Phys.* **1977**, *23*, 187−199.
(83) Valleau, J. P.; Torrie, G. M. A guide to Monte Carlo for statistical mechanics: 1. Highways. In *Modern Theoretical Chemistry*; Berne, B. J., Ed.; Plenum Press: New York, 1977; Vol. *5*, pp 169−194.
(84) Beutler, T. C.; Mark, A. E.; van Schaik, R.; Gerber, P. R.; van Gunsteren, W. F. *Chem. Phys. Lett.* **1994**, *222*, 529−539.
(85) Davis, M. E.; Madura, J. D.; Luty, B. A.; McCammon, J. A. *Comput. Phys. Commun.* **1991**, *62*, 187−197.
(86) Madura, J. D.; Briggs, J. M.; Wade, R. C.; Davis, M. E.; Luty, B. A.; Ilin, A.; Antosiewicz, J.; Gilson, M. K.; Bagheri, B.; Scott, L. R.; McCammon, J. A. *Comput. Phys. Commun.* **1995**, *91*, 57−95.
(87) Hünenberger, P. H.; McCammon, J. A. *J. Chem. Phys.* **1999**, *110*, 1856−1872.
(88) Peter, C.; van Gunsteren, W. F.; Hünenberger, P. H. *J. Chem. Phys.* **2002**, *116*, 7434−7451.
(89) Peter, C.; van Gunsteren, W. F.; Hünenberger, P. H. *J. Chem. Phys.* **2003**, *119*, 12205−12223.
(90) Ferrara, P.; Caflisch, A. *Proc. Natl. Acad. Sci. U.S.A.* **2000**, *97*, 10780−10785.
(91) Kastenholz, M.; Hünenberger, P. H. *J. Phys. Chem. B* **2004**, *108*, 774−788.
(92) Reif, M. M.; Kräutler, V.; Kastenholz, M. A.; Daura, X.; Hünenberger, P. H. *J. Phys. Chem. B* **2009**, *113*, 3112−3128.
(93) Ashbaugh, H. S.; Wood, R. H. *J. Phys. Chem. B* **1998**, *102*, 3844−3845.
(94) Malde, A. K.; Zuo, L.; Breeze, M.; Stroet, M.; Poger, D.; Nair, P. C.; Oostenbrink, C. *J. Chem. Theory Comput.* **2011**, *7*, 4026−4037.
(95) Jensen, K. P.; Jorgensen, W. L. *J. Chem. Theory Comput.* **2006**, *2*, 1499−1509.
(96) Turner, J. Z.; Soper, A. K.; Finney, J. L. *J. Chem. Phys.* **1995**, *102*, 5438−5443.
(97) Caminiti, R.; Cucca, P.; Monduzzi, M.; Saba, G. *J. Chem. Phys.* **1984**, *81*, 543−551.
(98) Mason, P. E.; Neilson, G. W.; Dempsey, C. E.; Barnes, A. C.; Cruickshank, J. M. *Proc. Natl. Acad. Sci. U.S.A.* **2003**, *100*, 4557−4561.
(99) Steiner, T. *Angew. Chem.* **2002**, *115*, 50−80.
(100) Kumar, S.; Bouzida, D.; Swendsen, R. H.; Kollman, P. A.; Rosenberg, J. M. *J. Comput. Chem.* **1992**, *13*, 1011−1021.
(101) Roux, B. *Comput. Phys. Commun.* **1994**, *91*, 275−282.
(102) Trzesniak, D.; Kunz, A.-P. E.; van Gunsteren, W. F. *Chem. Phys. Chem.* **2007**, *8*, 162−169.
(103) Bergdorf, M.; Peter, C.; Hünenberger, P. H. *J. Chem. Phys.* **2003**, *119*, 9129−9144.
(104) Baumketner, A. *J. Chem. Phys.* **2009**, *130*, 104106/1−104106/10.
(105) Churchill, C. D. M.; Wetmore, S. D. *J. Phys. Chem.* **2009**, *113*, 16046−16058.
(106) Singh, N. J.; Kyu Min, S.; Young Kim, D.; Kim, K. S. *J. Chem. Theory Comput.* **2009**, *5*, 515−529.
(107) Collins, K. D. *Methods* **2004**, *34*, 300−311.
(108) Hess, B.; van der Vegt, N. F. A. *Proc. Natl. Acad. Sci. U.S.A.* **2009**, *106*, 13296−13300.
(109) Gilson, M. K.; Honig, B. H. *Biopolymers* **1986**, *25*, 2097−2119.
(110) Warshel, A.; Sharma, P. K.; Kato, M.; Parson, W. W. *Biochim. Biophys. Acta* **2006**, *1764*, 1647−1676.
(111) Mellor, B. L.; Cortes, E. C.; Busath, D. D.; Mazzeo, B. A. *J. Phys. Chem. B* **2011**, *115*, 2205−2213.
(112) Albert, A.; Goldacre, R.; Phillips, J. *J. Chem. Soc.* **1948**, *Dec*, 2240−2249.
(113) Nozaki, Y.; Tanford, C. *J. Am. Chem. Soc.* **1967**, *89*, 736−742.
(114) IUPAC. *Biochemistry* **1970**, *9*, 3471−3479.